TOPICAL REVIEW

The structure of amorphous, crystalline and liquid GeO_2

INSTITUTE OF PHYSICS PUBLISHING JOURNAL OF PHYSICS: CONDENSED MATTER

J. Phys.: Condens. Matter **18** (2006) R753–R784 doi:10.1088/0953-8984/18/45/R01

TOPICAL REVIEW

The structure of amorphous, crystalline and liquid GeO_2

M Micoulaut[1], L Cormier[2] and G S Henderson[3]

[1] Laboratoire de Physique Théorique de la Matière Condensée, Université Pierre et Marie Curie, CNRS UMR 7600, Boite 121, 4 place Jussieu, 75252 Paris Cedex 05, France
[2] Institut de Minéralogie et de Physique des Milieux Condensés, Université Pierre et Marie Curie, Université Denis Diderot, CNRS UMR 7590, 4 place Jussieu, 75252 Paris Cedex 05, France
[3] Department of Geology, University of Toronto, 22 Russell Street, Toronto, ON M5S 3B1, Canada

Received 18 July 2006, in final form 12 September 2006
Published 26 October 2006
Online at stacks.iop.org/JPhysCM/18/R753

Abstract

Germanium dioxide (GeO_2) is a chemical analogue of SiO_2. Furthermore, it is also to some extent a structural analogue, as the low- and high-pressure short-range order (tetrahedral and octahedral) is the same. However, a number of differences exist. For example, the GeO_2 phase diagram exhibits a smaller number of polymorphs, and all three GeO_2 phases (crystalline, glass, liquid) have an increased sensitivity to pressure, undergoing pressure-induced changes at much lower pressures than their equivalent SiO_2 analogues. In addition, differences exist in GeO_2 glass in the medium-range order, resulting in the glass transition temperature of germania being much lower than for silica. This review highlights the structure of amorphous GeO_2 by different experimental (e.g., Raman and NMR spectroscopy, neutron and x-ray diffraction) and theoretical methods (e.g., classical molecular dynamics, *ab initio* calculations). It also addresses the structures of liquid and crystalline GeO_2, that have received much less attention. Furthermore, we compare and contrast the structures of GeO_2 and SiO_2, as well as along the GeO_2–SiO_2 join. It is probably a very timely review, as interest in this compound, that can be investigated in the liquid state at relatively low temperatures and pressures, continues to increase.

(Some figures in this article are in colour only in the electronic version)

Contents

1. Introduction

Zachariasen [1] proposed the continuous random network model (CRN) to explain the structure of oxide glasses, and it has subsequently received wide acceptance in describing glasses that form continuous random networks. To date the majority of studies of oxide glasses have involved the investigation of silica (SiO_2) or borate (B_2O_3) glasses with, to a lesser extent, germania (GeO_2) glasses. The structure of the latter has generally been considered to be comparable to that of silica glass despite differences in bond lengths, angles and the relative size of Ge versus Si. Experimental studies of amorphous GeO_2 have generally involved either x-ray or neutron scattering and spectroscopic techniques such as x-ray absorption spectroscopy (EXAFS/XANES) and Raman spectroscopy. On the other hand, theoretical studies have generally employed classical or *ab initio* molecular dynamics calculations to gain insight into the structure of these materials. In both approaches, the results of the studies are often compared to the known crystalline polymorphs of GeO_2. Here we review the structure of amorphous GeO_2 (glass and liquid) from both an experimental and a theoretical perspective, as well as comparing their structure with that of amorphous SiO_2 (glass, liquid). Furthermore, we review the structure of the crystalline GeO_2 polymorphs, both at room temperature and pressure and at elevated temperatures and pressures.

2. Crystalline GeO_2 polymorphs

2.1. Structure

Crystalline GeO_2 exists at ambient temperatures and pressures as one of two polymorphs (figure 1): an α-quartz-like ($P3_221$) trigonal (hexagonal) structure [2] or a rutile-like tetragonal ($P4_2/mnm$) structure [3].

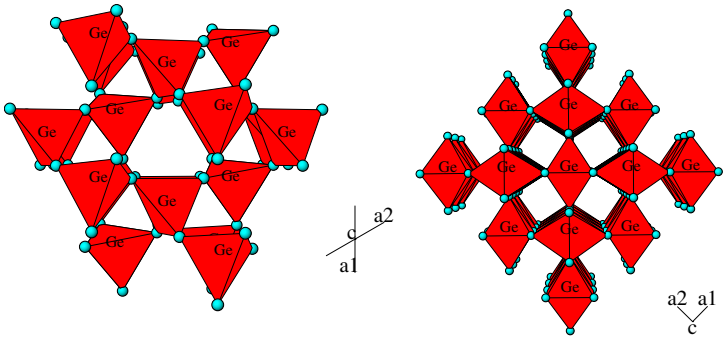

Figure 1. Projection of the α-quartz-like structure (left) and rutile-like structure (right) onto the (001) plane.

The α-quartz-like GeO_2 structure has been shown to be the stable high temperature phase [4] and, while the structure is very similar to that of α-quartz, there are some distinct differences. In particular the GeO_4 tetrahedra are more distorted due to greater variation in the O–Ge–O angles within the tetrahedron, which range from 106.3° to 113.1° with a Ge–O–Ge angle of 130.1°. This is in contrast to α-quartz where the O–Si–O angles within the SiO_4 tetrahedron are relatively uniform, ranging from 108.3° to 110.7° with a Si–O–Si angle of 144.0° [5]. These differences are important, as they result in different mechanisms being responsible for the high pressure behaviour of α-quartz and α-quartz-like GeO_2. For α-quartz the tetrahedra are relatively rigid and compression of the structure occurs via cooperative rotation or tilting of the tetrahedra around the shared bridging oxygens. Conversely, for α-quartz-like GeO_2, while compression does occur via tilting of the tetrahedra, distortion of each tetrahedron via changes in the individual O–Ge–O angles also plays a large role [5]. This behaviour is the reason why germanate analogues of silicate phases are useful in high pressure studies since they undergo pressure-induced phase transformations at much lower pressures than their silicate analogues. The transformation of α-quartz to the high pressure rutile structure (Stishovite) occurs at 10 GPa, while the equivalent transformation for α-quartz-like GeO_2 to rutile-like GeO_2 has been observed to occur at much lower pressures when the sample is heated: $\simeq$1.8–2.2 GPa at 417 K [6].

As noted above, the stable room temperature GeO_2 phase is the rutile GeO_2 polymorph, which transforms to the α-quartz-like structure at 1281 K ([4, 7] and references therein). The rutile GeO_2 polymorph has a structure similar to that of stishovite [3] and, like stishovite, the two axial bonds within the GeO_6 polyhedron are longer than the four equatorial Ge–O bonds: 1.902 ± 0.001 and 1.872 ± 0.001 Å, respectively. Conversely, the two independent Ge–O distances in the α-quartz-like GeO_2 structure are similar at 1.737 ± 0.003 and 1.741 ± 0.002 Å [2].

2.2. High pressure and temperature behaviour

A number of studies have investigated the high pressure behaviour of the two GeO_2 polymorphs. Itié *et al* [8] investigated α-quartz-like GeO_2 at ambient temperature. They observed an increase in the Ge–O bond length and Ge coordination number consistent with the formation of the rutile-like GeO_2 phase between 7 and 9 GPa. However, subsequent studies have suggested that the transformation is to an amorphous phase rather than the crystalline rutile-like GeO_2 polymorph [7, 9–11]. Furthermore, it has been suggested that the

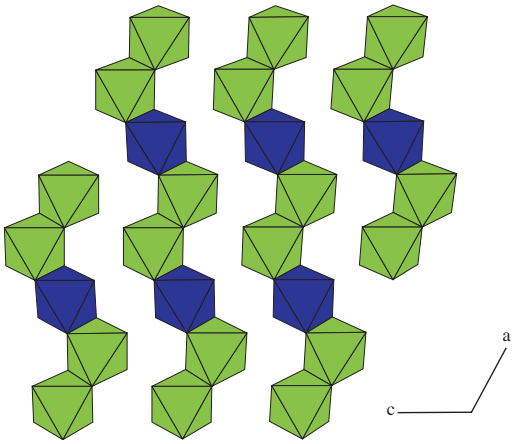

Figure 2. Polyhedral representation of the (3 × 2)-kinked $P2_1/c$ structure of GeO_2 determined by Haines *et al* [15]. Crystallographic axes are not to scale and are merely to show the orientation of the structure. Green (light) octahedra are the fully occupied Ge positions while the blue (dark) octahedra are the Ge octahedra which exhibit partial occupancy.

amorphization step is a precursor to subsequent transformation to the rutile polymorph [11]. More recently, Brazhkin *et al* [12–14] have shown that with compression α-GeO_2 changes via a martensitic transition into a crystalline monoclinic ($P2_1/c$) phase. On the other hand, Haines *et al* [15] suggest that there is no evidence for amorphization of the crystal. Instead, a poorly crystalline monoclinic ($P2_1/c$) phase forms, consisting of edge sharing chains of GeO_6 octahedra (figure 2).

The monoclinic phase is metastable up to 50 GPa. However, when combined with heating, it transforms to the rutile structure at pressures up to 22 GPa and above 43 GPa forms a mixture of $CaCl_2$-type and Fe_2N-type (or α-PbO_2, see later) high-pressure phases [12, 13, 15]. This monoclinic phase was also reported by Prakapenka *et al* [16] between 7 and 52 GPa at room temperature, but with laser heating it transforms to an orthorhombic $CaCl_2$-type structure above 36.4 GPa and an α-PbO_2-type structure at 41 GPa.

Haines *et al* [17] have also observed transformation of the rutile-like GeO_2 phase to the orthorhombic $CaCl_2$-type structure above 25 GPa at ambient temperature, while Ono *et al* [18] observed the transition at high pressure and temperature. *Ab initio* calculations by Lodziana *et al* [19] suggested that rutile-type GeO_2 should transform to α-PbO_2-type (above $\simeq$36 GPa) and pyrite- ($Pa\bar{3}$) type (above $\simeq$65.5 GPa) structures and these were subsequently observed by Ono *et al* [20, 21] around 44 and 90 GPa, respectively. An Fe_2N-type (or defect Ni As) phase at pressures larger than 25 GPa has been observed by Liu *et al* [22] and Haines *et al* [15]. This type of structure is similar to an α-PbO_2-type structure but with the Ge sites disordered and has, more recently, been explicitly identified by Ono *et al* [20] as being the α-PbO_2-type structure. However, it should be noted that Prakapenka *et al* [23] observe the defect NiAs structure when amorphous GeO_2 is heated to 1000–1300 K at 6 GPa (see later).

Structural refinements of the crystalline phases have been obtained by Shiraki *et al* [24] and a phase diagram for crystalline GeO_2 is given in figure 3. In addition, another orthorhombic phase has been suggested to occur at $\simeq$28 GPa and 1273 K by Ming and Manghnani [25]. They concluded that this phase was not the α-PbO_2-type structure but it has not been observed subsequently. The phase transformation sequence of rutile-like GeO_2 $\rightarrow$ (25 GPa) $CaCl_2$-type $\rightarrow$ (44 GPa) α-PbO_2-type $\rightarrow$ (70–90 GPa) pyrite-type structures is consistent with the

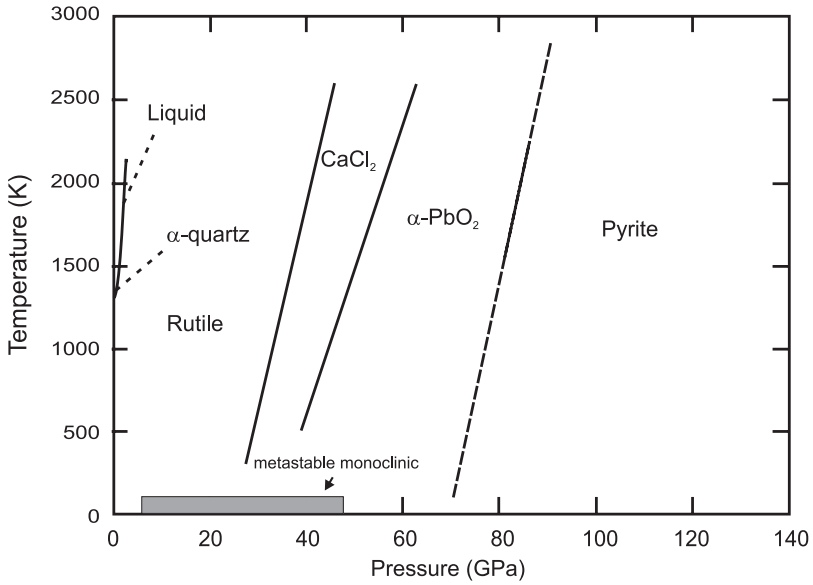

Figure 3. Phase diagram of crystalline GeO_2 (after [20]).

high-pressure behaviour of other group-IV element dioxides such as PbO_2, SnO_2, and SiO_2 (cf, [26, 19, 16, 23]).

Of interest is the way in which the α-quartz-like and rutile-like GeO_2 structures respond to increasing pressure. As noted above, Jorgensen [5] observed that in the α-quartz-like polymorph compression up to 2.5 GPa occurs predominantly via changes in the individual O–Ge–O angles and that tilting of tetrahedra was secondary. Yamanaka and Ogata [27] carried out a series of structural refinements on the α-quartz-like GeO_2 polymorph up to 4.48 GPa and found that the GeO_4 tetrahedra are relatively rigid with little change in the Ge–O bond length, consistent with the study of Itié *et al* [8]. Yamanaka and Ogata [27] found that the dominant mechanism responsible for the observed pressure-induced unit-cell volume change in the structure involved a decrease in the Ge–O–Ge angle from 130° to 125°. Conversely, Glinneman *et al* [28] found that tetrahedral tilting was responsible for the 11% volume change of α-quartz-like GeO_2 up to 5.57 GPa.

The phase transformation of rutile-like GeO_2 to the $CaCl_2$-type structure occurs via compression of the axial Ge–O bonds of the octahedron. The axial bonds are elongated relative to the equatorial bonds (see above). With increasing pressure there is increased compression of the axial relative to equatorial bonds [17] and the transformation at 25 GPa occurs during flattening of the octahedra [17, 24]. With transformation to the α-PbO_2-type structure, the GeO_6 octahedron becomes further deformed with the Ge atom displaced from the centre of the octahedron and two of the six Ge–O bonds becoming elongated [24], as suggested by the numerical results of Lodziana *et al* [19]. Transformation to the pyrite-type structure, however, results in GeO_6 octahedra that are symmetrical with Ge in the centre.

As noted above, the α-quartz-like polymorph is the stable high-temperature phase and rutile-type GeO_2 will transform to this polymorph above 1320 K, the transformation temperature being the highest of any of the quartz-like analogues. The high-temperature (up to 1344 K) behaviour of this polymorph has been investigated by Haines *et al* [29], who found that the intertetrahedral bridging angle (Ge–O–Ge) and tilt angles exhibit thermal

stabilities that are amongst the highest observed for quartz-type analogues. With increasing temperature, expansion of the unit cell is highly anisotropic, with expansion along **a** being five times greater than along **c** [29]. However, the α-quartz-like GeO_2 polymorph is metastable at low temperatures ([30] provide a number of methods for growing the α-quartz-like GeO_2 polymorph), but does undergo transformation to the rutile-type polymorph at around 1000 K, although the reaction proceeds slowly due to the kinetics involved (cf [31]). Finally, it should be noted that a cristobalite-like polymorph for GeO_2 has been observed after long-time heating of GeO_2 glass to 873 K [32] or by dehydration of ammonium hydrogen germanate ($(NH_4)_3HGe_7O_{16.4}H_2O$) between 853 and 873 K [33]; however, this polymorph has not been observed in *in situ* high-pressure and temperature studies. In addition, the β-quartz-like polymorph at 1322 K mentioned by Leadbetter and Wright [34] and Desa *et al* [35] based on the work of Laubengayer and Morton [4] and Sarver and Hummel [36] has also not been observed.

3. GeO_2 glass structure

3.1. Neutron and x-ray diffraction

Neutron and x-ray diffraction data are complementary tools for inferring structural information since the chemical sensitivity is different for the two techniques; Ge–O and Ge–Ge pairs are better resolved with x-rays and Ge–O and O–O with neutrons.

GeO_2 glass structure has been studied using x-ray diffraction in the pioneering work of Warren [37], [38] and Zarzycki [39], [40]. It was found that the Ge atoms are arranged in basic tetrahedral units such as those found in the trigonal α-quartz-like GeO_2 polymorph. X-ray diffraction data with higher real space resolution ($Q_{max} = 17$ Å^{-1}) confirmed these findings [34] and determined the first Ge–O and Ge–Ge distances at 1.74 and 3.18 Å, respectively, giving an intertetrahedral angle of $\simeq$133°. The first neutron diffraction experiment ($Q_{max} = 18$ Å^{-1}) on vitreous GeO_2 shows two strong peaks at 1.72 and 2.85 Å ascribed to Ge–O and O–O correlations, which is consistent with GeO_4 tetrahedra [41]. The Ge–Ge peak, initially determined at 3.45 Å [41, 42], was resolved in a high-resolution neutron diffraction investigation ($Q_{max} = 35.5$ Å^{-1}) at 3.21 Å, which is slightly higher than the Ge–Ge distance determined by x-ray diffraction due to the overlapping of Ge–O and O–O pairs [43, 44]. A recent neutron and x-ray diffraction investigation [35] has shown that the O–Ge–O intratetrahedral angle is more distorted in vitreous GeO_2 than in vitreous SiO_2, with a distribution probably comparable to that of GeO_2 α-quartz (106.3°–113.1°). This is due to the larger radius of Ge than Si, allowing more accessible positions for O atoms around Ge atoms. The mean Ge–O–Ge intertetrahedral angle was estimated from the Ge–O and Ge–Ge distances to be 130.1° with a range of 121°–147°. This mean value was confirmed at 133$\pm$8.3° using high-energy x-ray diffraction [45]. This bond angle and its distribution are lower than in the case of vitreous silica. The smaller Ge–O–Ge angle probably results from the presence of increased numbers of three-membered rings in the GeO_2 network relative to vitreous SiO_2 (cf [35] and see later) since such planar rings have a Ge–O–Ge angle of 130.5° [46, 47]. The values for the main interatomic distances, coordination numbers and intertetrahedral angles found in these studies are reported in table 1. The structure of GeO_2 can thus be viewed as a continuous random network of corner sharing tetrahedra as in silica, but with greater distortion of the tetrahedra and larger numbers of three-membered rings.

The diffraction data (figure 4) of GeO_2 are composed of three partial functions, Ge–Ge, Ge–O and O–O. The first attempt to separate the three components was carried out using x-ray anomalous diffraction and neutron diffraction [48, 49]. The Ge–O, O–O and Ge–Ge

Table 1. Interatomic distances (R), coordination numbers (N), standard deviations (σ) and Ge–O–Ge intertetrahedral angle determined by diffraction methods. (1) $Q_{max} = 50$ Å^{-1}, [57]; (2) $Q_{max} = 50$ Å^{-1}, [62]; (3) $Q_{max} = 9$ Å^{-1}, [51]; (4) [53]; (5) 1 Å$^{-1} \leqslant Q \leqslant 10$ Å^{-1}, [50]; (6) 0.6 Å$^{-1} \leqslant Q \leqslant 33.5$ Å^{-1}, [45]; (7) 0.22 Å$^{-1} \leqslant Q \leqslant 23.6$ Å^{-1}, [35]; (8) [49]; (9) 0.8 Å$^{-1} \leqslant Q \leqslant 17$ Å^{-1}, [34]. ND = neutron diffraction; AXS = anomalous x-ray scattering; HEXRD = high energy x-ray diffraction; XRD = x-ray diffraction.

Pair ij	R (Å)	N	σ (Å)	Method	Reference
Ge–O	1.733 ± 0.001	3.99 ± 0.1	0.042 ± 0.001	ND	(1)
	1.744 ± 0.05	4.0 ± 0.2	0.11 ± 0.01	ND	(2)
	1.73 ± 0.03			ND+AXS	(3)
	1.74 ± 0.01	3.7 ± 0.2		ND	(4)
	1.75			ND+AXS	(5)
	1.73			HEXRD	(6)
	1.739 ± 0.005	3.9 ± 0.1		D	(7)
	1.73			AXS	(8)
	1.74			XRD	(9)
O–O	2.822 ± 0.002	6.0[a]	0.100 ± 0.002	ND	(1)
	2.84 ± 0.01	6.0 ± 0.3	0.26 ± 0.03	ND	(2)
	2.83 ± 0.05			ND+AXS	(3)
	2.84 ± 0.02	5.5 ± 0.5		ND	(4)
	2.82			ND+AXS	(5)
	2.838	6.0[a]	0.109	ND	(7)
Ge–Ge	3.155 ± 0.01	4.0 ± 0.3	0.26 ± 0.03	ND	(2)
	3.16 ± 0.03			ND+AXS	(3)
	3.18 ± 0.05			ND	(4)
	3.18			ND+AXS	(5)
	3.17			HEXRD	(6)
	3.185	4.0[a]	0.163	ND	(7)
	3.17			AXS	(8)
	3.18			XRD	(9)
Angle	Ge–O–Ge				
	$132 \pm 5°$			ND+AXS	(3)
	$133 \pm 8.3°$			HEXRD	(6)
	130.1°			ND+XRD	(7)
	133°			XRD	(9)

[a] Fixed values.

distances are found at 1.73, 2.85 and 3.17 ± 0.04 Å, respectively, and the average Ge–O–Ge intertetrahedral bond angle is estimated to have values between 129° and 139°. Recently, by combining neutron and x-ray diffraction, together with x-ray anomalous scattering, the three partial functions were fully separated up to $Q = 9$ Å^{-1} [50, 51], though problems exist due to different instrumental resolution functions that appear especially at low Q values, and the necessity to improve the anomalous scattering terms [52]. The structure factors are dominated by peaks occurring at 1.54, 2.6 and $\simeq$4.5 Å^{-1}. The first feature at 1.54 Å^{-1} (usually called first sharp diffraction peak, FSDP) corresponds to intermediate-range ordering and is stronger in x-ray than in neutron data [53]. The FSDP is associated with a positive peak in S_{GeGe} and S_{GeO} and a shallow negative peak in S_{OO}, indicating that cation correlations dominate the medium-range order (figure 5, [51]). The peak at 2.6 Å^{-1} is strong and positive in S_{GeGe} and S_{OO}, and strong and negative in S_{GeO}, and has been attributed to chemical short-range order. The peak at 4.4 Å^{-1} occurs predominantly in S_{GeGe} and is due to topological short-range order. The latter conclusion is usually extracted from Bhatia–Thornton structure factors [54] that show

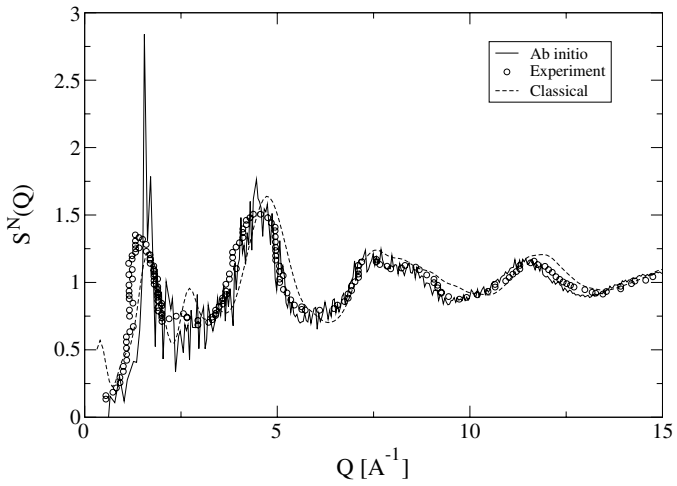

Figure 4. Measured total structure factor (circles, [57]) together with calculated $S(Q)$ from *ab initio* (solid line, [58]) and classical molecular dynamics (broken line, [59]).

the correlations between number density and concentration fluctuations [55]. On this basis, the chemical and topological ordering in GeO_2 can be rationalized in terms of an interplay between the relative importances of two length-scales that exist in the glass [56].

There have been considerable efforts to compare diffraction data obtained on GeO_2 glass with equivalent calculations based on the GeO_2 crystalline polymorphs, with divergent results. Leadbetter and Wright [34] concluded that the intermediate range order in the glass closely resembles a quasi-crystalline model based on the α-quartz-like GeO_2 structure with a correlation length of 10.5 Å but discrepancies appear beyond 4 Å. Bondot [49] obtained good agreement between the glass and the α- and β-quartz GeO_2 polymorphs, which led to the conclusion that the glass contains six-membered rings. In contrast, Konnert *et al* [61] concluded that vitreous germania, like vitreous silica, possesses the same short-range order as that found in the tridymite SiO_2 polymorph. The vitreous GeO_2 structure could thus be described as randomly oriented, slightly distorted tridymite-like regions having dimensions ranging up to at least 20 Å [61]. However, these regions are not crystallographically ordered (i.e. not microcystals) but have similar bonding topology in the glass and in tridymite. In a more recent study [35], it was shown that, though similarities exist with crystalline α-quartz-like and α-cristobalite-like GeO_2 polymorphs, diffraction data are not consistent with large volume fractions of quasi-crystalline-like regions, due to an important distribution of torsion angles.

3.2. Neutron and x-ray diffraction at high pressure and temperature

Due to the technical difficulties associated with performing *in situ* diffraction experiments, pressure effects have been mainly studied on pressure-released glasses, in which permanent densification is observed. Permanently densified glasses (up to 18 GPa) were studied by x-ray diffraction in the low-Q region (FSDP), which is sensitive to medium-range order [63]. A shift to higher Q and an increase in width of the FSDP is observed above 6 GPa, a pressure corresponding to the threshold for coordination changes observed in *in situ* experiments (see below). However, comments on this study pointed out that changes in the diffraction peaks may not necessarily be associated with a coordination change [64].

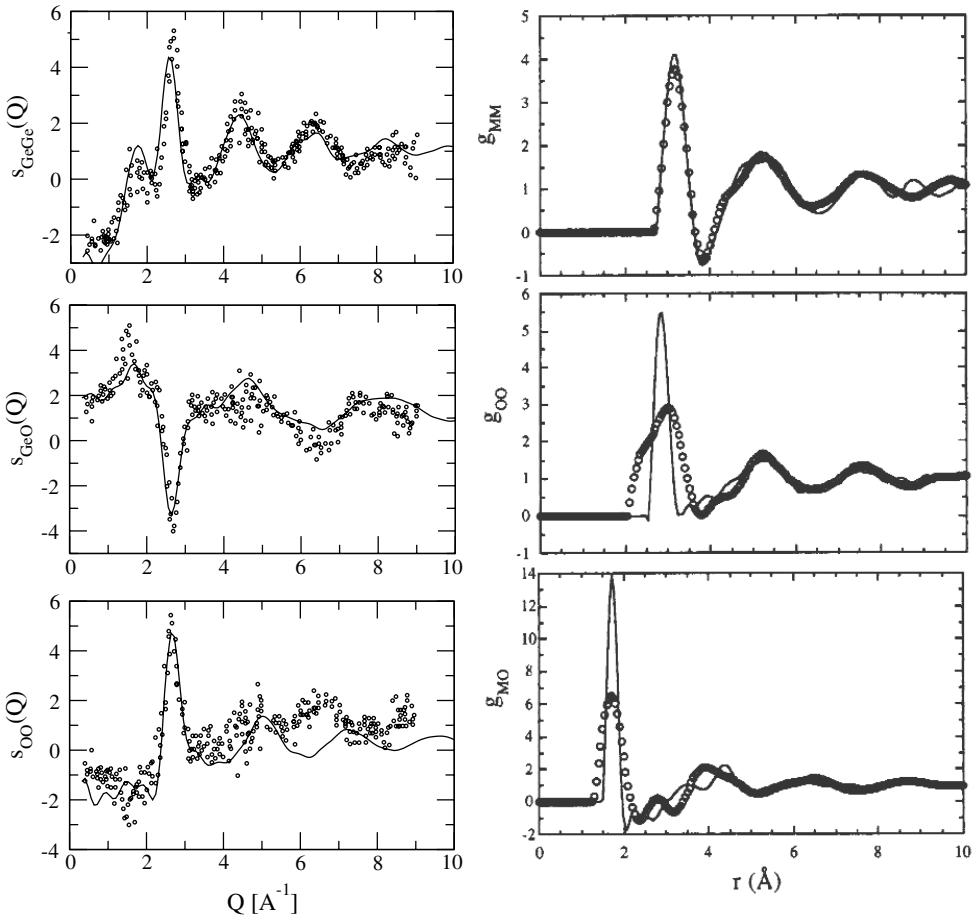

Figure 5. Left from top to bottom: measured (circles, [51]) and calculated (solid line, [60]) partial structure factors, $S_{GeGe}(Q)$, $S_{GeO}(Q)$ and $S_{OO}(Q)$. Right: partial correlation functions, $g_{MM}(r)$, $g_{MO}(r)$ and $g_{OO}(r)$ (from top to bottom), for the three atom pairs in vitreous GeO_2 at room temperature (M = Ge, points), together with the corresponding functions from rescaled molecular dynamics simulation of vitreous SiO_2 (M = Si, lines) (after [51]).

GeO_2 glasses densified up to 6 GPa at 673 K (densification of 16%) were investigated by neutron diffraction [57], while a glass densified at 10 GPa and 300 K (densification of 11%) was studied by neutron and x-ray diffraction (figure 6) [65]. No evidence of six-coordinated Ge was observed. The GeO_4 tetrahedra are distorted, with Ge–O distances increasing by 0.005 ± 0.001 Å and O–O and Ge–Ge distances decreasing by 0.023 ± 0.002 and 0.019 ± 0.002 Å, respectively [65]. The main change is a shift of the Ge–Ge peak (at $\simeq$3.1 Å) to lower r values with increasing pressure compaction [57]. This indicates a reduction in the mean Ge–O–Ge bond angle with increasing density. Noticeable changes are seen for the FSDP in the neutron and x-ray structure factors: the FSDP shifts towards higher Q, broadens and becomes less intense on densification. This indicates a reduction of the network connectivity. By combining neutron and x-ray diffraction up to $Q = 30$ Å^{-1}, it was shown [65] that variations of the FSDP are mostly associated with O–O correlations rather than Ge–Ge ones. This is attributed to a decrease in the average size of the network cages (these can be considered

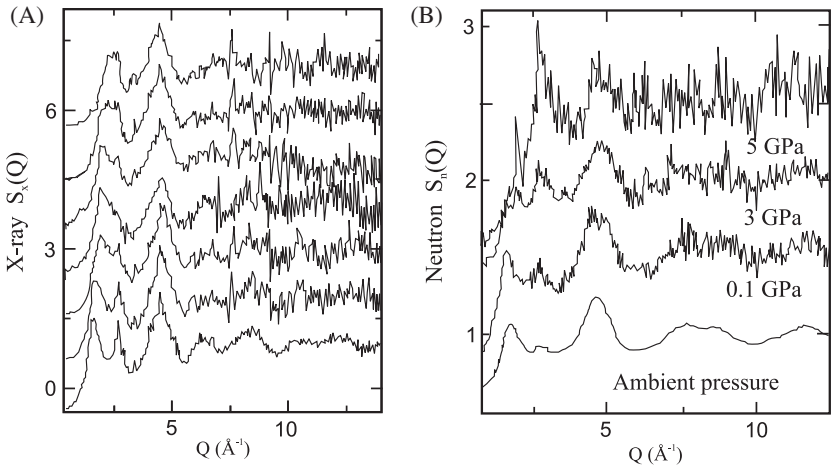

Figure 6. *In situ* structure factors (after [66]) for (A) x-ray diffraction at 0, 3, 5, 6, 7, 10 and 15 GPa (bottom to top) and (B) neutron diffraction up to 5 GPa, with ambient-pressure data from Sampath *et al* [65].

as holes in the structures, formed for instance by the ring structures), yielding better packing of the GeO_4 tetrahedra.

In situ measurements have recently been obtained (figure 6) by both neutron (up to 5 GPa) and x-ray (up to 15 GPa) diffraction [66]. The FSDP decreases and almost vanishes with increasing pressure in neutron measurements while it gradually shifts to higher Q in x-ray data. This is interpreted as a breakdown of the intermediate-range order upon compaction of the tetrahedral network associated with changes in the oxygen correlations. In the x-ray correlation functions, a reduction of the Ge–O distance is observed below 6 GPa while it increases at further pressure, corresponding to GeO_4 tetrahedra being converted to GeO_6 octahedra. Based on molecular dynamics simulations, it was argued that stable fivefold units are present in the transition region, indicating a new intermediate form of the glass. The structure of the high-pressure glass is based on edge- and corner-shared octahedra, which is not retained upon decompression.

GeO_2 in the liquid state has been investigated by x-ray diffraction [40, 67]. The Ge–O distance is unchanged, in agreement with a small thermal expansion of the Ge–O bond similar to that for Si–O bonds. The GeO_4 tetrahedra are preserved in the GeO_2 melt but Ge–Ge distances are shifted from 3.16 Å at room temperature to 3.25 Å at 1100 °C, which is interpreted as a widening of the Ge–O–Ge bond angle.

3.3. Raman spectroscopy

3.3.1. GeO_2 polymorphs. The Raman spectra of the crystalline polymorphs of GeO_2 (figure 7) were first reported by Scott [68]. The rutile-like GeO_2 spectrum exhibits three strong bands in the 150–1200 cm^{-1} range at 173, 701 and 873 cm^{-1}. The band at 701 cm^{-1} is the A_{1g} mode while the 873 cm^{-1} band is the B_{2g} mode. The B_{1g} mode is at 173 cm^{-1}. The E_g mode observed at 680 cm^{-1} by Scott [68] is not observed in the spectrum shown in figure 7. Alpha-quartz-like GeO_2 has a number of additional bands including four symmetric modes of A_1 symmetry and eight doubly degenerate modes of E symmetry all split into transverse optic (TO) and longitudinal optic modes (LO) [68]. The α-quartz-like GeO_2 spectrum of figure 7 is comparable to that first obtained by Scott [68]. Bands can be assigned following Scott [68] and Dultz *et al* [69] as A_1 modes at 263, 330, 444, and 881 cm^{-1}; E modes at 123 (TO+LO), 166

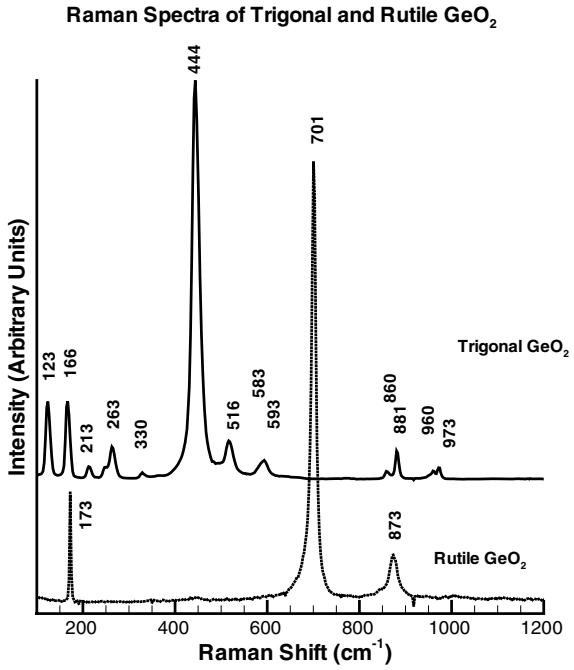

Figure 7. Unpolarized Raman spectra of the α-quartz-like and rutile-like GeO_2 polymorphs. Bands are comparable to those of Scott [68] and Madon *et al* [31]. For clarity not all bands are labelled.

(TO+LO), 212 (TO), 330 (TO), 516 (LO), 593 (LO), 860 (TO), 960 (TO), and 973 cm^{-1} (LO). E modes at 372 (LO), 385 (TO), 492 (TO), 583 (TO) and 949 cm^{-1} (LO) are too weak to be observed in the spectrum or are unlabelled for clarity.

The effects of increasing pressure and temperature on the vibrational spectra of the GeO_2 polymorphs has been investigated by Sharma [70], Madon *et al* [31] and Mernagh and Liu [71]. With increasing pressure the Raman bands for the α-quartz-like polymorph shift to higher wavenumber and behave in a similar manner as the IR modes [31]. The mean frequency shift is $\simeq$1 cm^{-1}/0.1 GPa for bands in the 400–600 cm^{-1} region and 0.3 cm^{-1}/0.1 GPa for the bands in the 100–330 cm^{-1} region, and the bands in the 850–970 cm^{-1} region do not shift at all up to 4 GPa except for the band at 961 cm^{-1}. The rutile Raman bands behave slightly differently [70], with the band at $\simeq$173 cm^{-1} shifting to lower wavenumbers and the other two bands to higher wavenumbers. With increasing temperature, the Raman bands of the rutile-like polymorph transform to the α-quartz-like spectrum at $\simeq$1313 K [31] while the Raman bands of the α-quartz-like polymorph show a nonlinear shift with increasing temperature. Madon *et al* [31] observed a shift of -0.01 cm^{-1} K^{-1} for the bands in the low-frequency region and -0.024 cm^{-1} K^{-1} in the mid- and high-frequency regions. For the rutile polymorph, the Raman bands above 600 cm^{-1} exhibit nonlinear shifts to lower wavenumbers, whereas the 173 cm^{-1} band exhibits a shift to higher wavenumbers with increasing T [71]. In addition, Mernagh and Liu [71] detect (by deconvolution) splitting of the A_{1g} mode (701 cm^{-1}) of the rutile-like polymorph with a new band observed at 684 cm^{-1}.

3.3.2. GeO_2 glass and liquid. The first Raman spectrum of GeO_2 glass was described by Bobovich and Tolub [72] and Obukhov-Denisov *et al* [73]. A Raman spectrum for GeO_2 glass is shown in figure 8(a). The Raman band assignments for GeO_2 glass are similar to those of

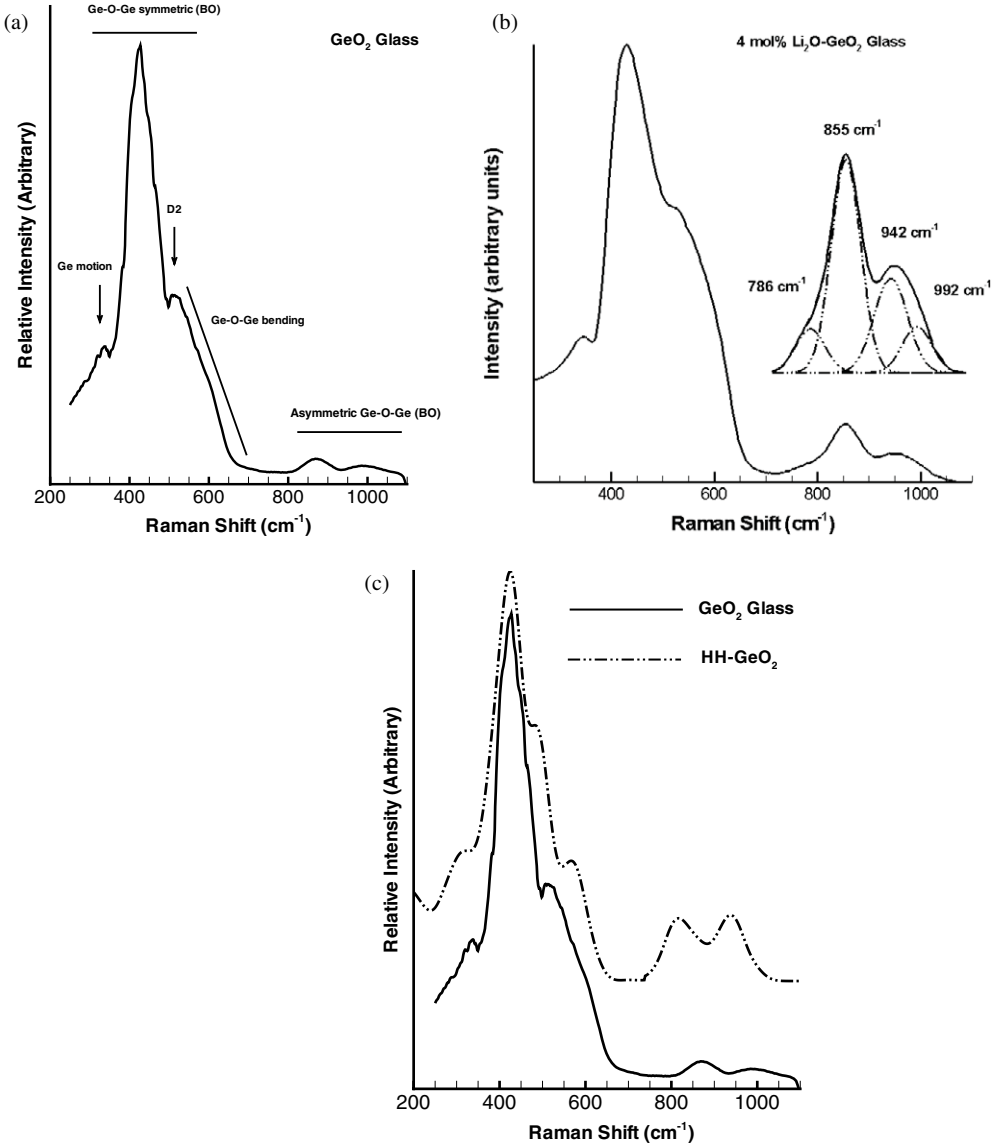

Figure 8. (a) Unpolarized Raman spectrum of GeO_2 glass showing the main vibrational bands, (b) a Raman spectrum of a Li_2O-containing germanate glass showing the high-frequency BO and NBO bands: the inset is a curve fit (deconvolution) of the high frequency envelope into its discrete vibrational bands (see table 2), (c) Unpolarized Raman spectrum of GeO_2 glass (solid line) compared with calculated HH spectrum of GeO_2 glass (dashed–dot line) from Giacomazzi *et al* [58]. The calculated spectrum has been shifted so that the main vibrational band is coincident with the equivalent band of the experimental spectrum.

SiO_2 glass but are shifted to lower frequencies (wavenumbers, cm^{-1}) because of the larger mass of Ge relative to Si. Currently accepted band assignments for GeO_2 are given in table 2 and extensive discussion of Raman assignments and earlier literature can be found in [74, 75].

The high-frequency bands observed at $\simeq$860 and 998 cm^{-1} are the TO and LO split asymmetric stretching bands of the bridging oxygens (Ge–O–Ge). The Ge–O–Ge bending

Table 2. Raman band assignments for GeO_2 glass and for the different Q species observed upon addition of a network modifier such as an alkali or alkaline-earth cation.

Frequency	Attribution
$\simeq$60 cm^{-1}	Boson peak; acoustic mode? Related to glass fragility
347 cm^{-1} (D_1)	Ge '*deformation*' motion within the network
420 cm^{-1}	Symmetric stretching of bridging oxygens (BO) in 6-membered GeO_4 rings: Ge–O–Ge
520 cm^{-1} (D_2)	'*Defect*' mode assigned to breathing motion of bridging oxygens in 3-membered GeO_4 rings
500–620 cm^{-1}	Bending modes: Ge–O–Ge, TO (556 cm^{-1}) and LO split (595 cm^{-1})
$\simeq$860 cm^{-1}	TO asymmetric stretching of bridging oxygens: Ge–O–Ge (Q^4)
$\simeq$988 cm^{-1}	LO asymmetric stretching of bridging oxygens: Ge–O–Ge (Q^4)
Q species vibrations	NBO (non-bridging oxygen) vibrations that occur upon addition of network modifiers such as alkalis
$\simeq$865 cm^{-1}	Q^3 GeO_4 tetrahedra with 3 BO and 1 NBO
780 cm^{-1}	Q^2 GeO_4 tetrahedra with 2 BO and 2 NBO

modes are observed in the broad region between $\simeq$500 and 620 cm^{-1} and have also been assigned to TO ($\simeq$556 cm^{-1}) and LO ($\simeq$595 cm^{-1}) split modes associated with significant Ge and O motion [76]. A '*defect*' band D_2 occurs at $\simeq$520 cm^{-1}. This defect mode is the equivalent of the D_2 band observed in SiO_2 glass at 606 cm^{-1} and is assigned similarly to an oxygen-breathing mode associated with three-membered rings of GeO_4 tetrahedra, and this assignment has been recently supported by the study of Giacomazzi *et al* [58] (figure 8(c)). The intensity of this band is much stronger relative to the main vibrational band at $\simeq$420 cm^{-1} in comparison to the equivalent bands for SiO_2 glass. This indicates that the GeO_2 network, while being composed predominantly of six-membered rings of GeO_4 tetrahedra (see above), does have a larger proportion of three-membered rings relative to SiO_2 glass. The relatively narrow band at around 420 cm^{-1} is the symmetric stretching mode of the Ge–O–Ge bridging oxygens. Its width is much narrower than the equivalent band observed in SiO_2 glass at 440 cm^{-1} and indicates that the distribution of Ge–O–Ge intertetrahedral angles for GeO_2 glass is narrower than that for SiO_2 glass consistent with the neutron and x-ray data above.

The origin of the boson peak (BP) at 60 cm^{-1} (the peak occurs over a broad range between 40–60 cm^{-1}) remains controversial. It has been assigned to acoustic-like harmonic modes, localized quasi-harmonic modes and the smallest-energy van Hove singularity of the crystal (cf [77, 78] and references therein). Most recently, there seems to be a consensus that the origin of the BP is due to optic-like excitations related to nearly rigid SiO_4 (or GeO_4) librations through hybridization of the acoustic waves [79]. It exhibits a dependence on the fragility of the glass (fragile glasses have weak BP intensity), as well as fictive temperature (for SiO_2 the BP shifts to higher wavenumber with increasing fictive temperature). In addition, there is a monotonic frequency shift in the BP for pure SiO_2, to lower wavenumbers with the addition of GeO_2, which may indicate that GeO_2 substitutes isomorphously into SiO_2 [78].

The Raman spectrum of GeO_2 glass indicates that the T–O–T intertetrahedral angle and its distribution are narrower for GeO_2 glass relative to SiO_2 glass, consistent with the x-ray and neutron diffraction studies (see above). These latter studies also suggest that the medium-range structure of GeO_2 glass consists of six-membered rings of GeO_4 tetrahedra, similar to those observed in the α-quartz polymorph of GeO_2, with a high proportion of small three-membered GeO_4 rings (relative to SiO_2 glass). An interesting aspect of the medium-range structure was raised by Henderson *et al* [74] and Henderson and Fleet [75] using Raman

spectroscopy. They suggested that the medium-range structure of GeO_2 may actually consist of four- rather than six-membered GeO_4 rings. This suggestion has not been explored further and there have not been any x-ray or neutron scattering studies that have compared GeO_2 glass with structures containing predominantly four-membered GeO_4 rings. However, Giacomazzi *et al* [58] recently used a model GeO_2 structure that had exclusively three- and four-membered GeO_4 rings. Their model reproduced the first sharp diffraction peak in the neutron static structure factor (indicative of medium range structure), and the infrared and Raman spectra of GeO_2 glass (figure 8(c)) reasonably well. The question of whether or not the medium-range structure of GeO_2 glass consists of six- or four-membered rings remains unanswered and open for further studies.

3.4. Infra-red (IR) spectroscopy

There have been relatively few infra-red studies of GeO_2 glass, primarily because the IR spectra are more difficult to interpret and obtain than the Raman spectra. One of the earliest is that of Kaiser *et al* [80], while more recent studies have tended to use IR in high-pressure studies [81] for investigating the onset of amorphous to amorphous phase transitions (see below). The IR spectrum of GeO_2 glass exhibits two peaks at 560 cm^{-1} and one at $\simeq$870 cm^{-1} with a shoulder at $\simeq$1000 cm^{-1}, although the relative intensities for these two bands are reversed in the spectra of Galeener *et al* [82]. The low frequency band at 560 cm^{-1} is the IR equivalent of the LO bending mode observed in the Raman spectrum at $\simeq$595 cm^{-1}, while the bands at 870 cm^{-1} and $\simeq$1000 cm^{-1} are the IR equivalent TO (870 cm^{-1}) and LO split asymmetric stretching of the bridging oxygens [82]. The data of Galeener *et al* [82] also show a peak in their IR reflectance spectrum at $\simeq$340 cm^{-1}, which is the equivalent of the 347 cm^{-1} Raman band. Galeener *et al* [82] assign this band however to an LO mode. In general the LO modes are more intense in the IR relative to Raman spectra, while the TO modes are more intense in the Raman relative to IR spectra.

With increasing pressure, the 560 and 870 cm^{-1} peaks broaden and the region between the bands ($\simeq$700 cm^{-1}) exhibits an increase in intensity [81], although part of this increase is due to a shift in the 560 cm^{-1} band to higher wavenumbers with increasing pressure (up to 6 GPa). Teredesai *et al* [81] also observe with increasing pressure a decrease in wavenumber for both high wavenumber bands. Above 6 GPa, all bands shift to higher wavenumbers coincident with the onset of the pressure-induced coordination change of Ge noted by Itié *et al* [8]. However, glasses decompressed from 9.5 GPa exhibit a 30 cm^{-1} red shift in the position of the 870 cm^{-1} peak with no shift in position of the 560 cm^{-1} peak [81].

3.5. Increasing pressure and temperature

The effect of pressure on GeO_2 glass at ambient temperature has been investigated by Ishihara *et al* [83] and *in situ* by Durben and Wolf [84] and Polsky *et al* [85]. Up to 6 GPa, Durben and Wolf [84] observe a shift of the main Raman band at $\simeq$420 cm^{-1} to higher frequency with concomitant broadening and loss of intensity. Between 6 and 13 GPa the main Raman band broadens and loses intensity without a shift in frequency. In addition, they observe the growth of a broad low-frequency band at $\simeq$240 cm^{-1} and no further spectral changes are observed beyond 13 GPa up to 56 GPa. However, upon decompression, the 520 cm^{-1} D_2 band characteristic of three-membered rings is enhanced relative to uncompressed GeO_2 glass and indicates that three-membered rings are formed during decompression from high pressure. Similar results were obtained by Polsky *et al* [85] and both they and Durben and Wolf [84] observe subtle changes in the Raman spectra between 5 and 10 GPa characteristic of the pressure-induced change in Ge coordination observed by *in situ* EXAFS and XANES studies [8].

Up to 5 GPa, both Durban and Wolf [84] and Polsky *et al* [85] suggest that compression of the GeO_2 glass network is taken up by tetrahedral deformation with a smaller decrease in the intertetrahedral angle. In addition, they conclude that there is no increase in intensity of the 520 cm^{-1} D_2 band. However, this conclusion is questionable given that the main Raman band at 420 cm^{-1} appears to move to higher wavenumbers with increasing pressure (above 4 GPa), and as Polsky *et al* [85] themselves note any apparent decrease in the intensity of the 520 cm^{-1} band may simply be a consequence of changes in the adjacent band at 420 cm^{-1}. Examination of figure 2 of Durben and Wolf [84] shows that above 3.7 GPa the 420 and 520 cm^{-1} bands are merged and individual bands are unable to be discriminated. Below 3.7 GPa, the intensity of the D_2 band also cannot be determined without some knowledge of how the spectra have been normalized but a cursory examination appears to indicate that the D_2 intensity has increased relative to the maximum in the main 420 cm^{-1} band. Furthermore, Ishihara *et al* [83], albeit using permanently densified GeO_2 glasses, note that growth of the D_2 band correlates with increasing pressure; higher pressures produce increased D_2 intensity although there are no permanent structural changes for glasses decompressed from below 4 GPa [85].

High temperature studies have been performed by Magruder *et al* [86] and Sharma *et al* [87]. With increasing temperature Magruder *et al* determined that the high-frequency TO/LO split pair undergoes a twofold loss of intensity between 1723 and 2023 K and that the D_2 band intensity remains constant. The high-frequency LO band at 988 cm^{-1} (figure 7(a)) loses intensity as the TO/LO splitting is lost with increasing temperature [87] but even in the melt phase two bands are observed at $\simeq$818 and 940 cm^{-1}, respectively. However, Sharma *et al* [87] observed an increase in intensity of the D_2 band and a shift of the main Raman band at 420 cm^{-1} to higher wavenumbers combined with a loss of intensity, while the low-frequency band at 347 cm^{-1} shifts to lower wavenumbers but is observed up to 1623 K. Both studies clearly show that the Raman bands observed in GeO_2 glass remain even in to the melt phase but that there are subtle changes in intensities and band positions as the glass is heated and eventually melts.

3.6. NMR spectroscopy

The coordination environment of Ge in GeO_2 and alkali-containing GeO_2 glasses remains an area of intense interest from a glass perspective because of the unusual physical properties of alkali-containing germanate glasses and the possible role of Ge coordination in this behaviour [75, 88]. Ge NMR would normally be the technique of choice to investigate the coordination environment of Ge in glasses. Germanium has five naturally occurring isotopes (^{70}Ge, ^{72}Ge, ^{73}Ge, ^{74}Ge and ^{76}Ge) but only ^{73}Ge is suitable for NMR studies. However, while ^{73}Ge NMR has been successfully performed on solid crystalline compounds [89–91] it has not been useful for elucidating the structure of glasses [92, 93].

The ^{17}O MAS NMR spectra of GeO_2 glass, and the α-quartz-like and rutile-like polymorphs of crystalline GeO_2, have been obtained by Du and Stebbins [93]. The two crystalline polymorphs and GeO_2 glass all exhibit a single crystallographic oxygen site similar to previous data obtained at lower magnetic fields [94]. The oxygen site in the GeO_2 glass is comparable to that found in the α-quartz-like GeO_2 polymorph, indicating that the glass consists of a network of GeO_4 tetrahedra, consistent with x-ray and neutron scattering studies.

4. Structure of densified liquid GeO_2

Melting curves at elevated pressures were first reported by Jackson [95] in the range 1100–1700 °C and 0.5–2 GPa. The high-temperature part of the phase diagram was also studied in [96], where an observed flattening of the melting curve at $P \simeq$ 2–4 GPa seems to be an

indication of densification of the melt due to the transformation of a quartz-like liquid into a rutile-like one.

Ordering of the melt structure in the same range of temperatures and pressures as above was also reported [97] from Raman scattering. Specifically, the lowering of the Rayleigh line intensity from *in situ* high-pressure and temperature liquid Raman spectra was found to be significantly lower than for a glass quenched at ambient pressure. This suggests an increased degree of short-range order on compression in the liquid and a more ordered network structure. However, it constitutes a major obstacle to studying liquid GeO_2 at elevated pressures. Note that molecular dynamics has not tried to simulate these experiments yet (see below).

5. Structure of the binary SiO_2–GeO_2 glasses

Germania and silica are prototype glasses for continuous random network models, based on the corner sharing connection of their SiO_4 and GeO_4 tetrahedra. The variations in the intertetrahedral angles and the presence of some structural defects (for instance dangling bonds in SiO_2 glass) allows the formation of a three-dimensional disordered network.

Germanosilicate glasses are widely used as low-attenuation optical fibres, yielding numerous studies on their physical (optical) properties [98]. Structural studies are more scarce, despite the need for an understanding of the relationship between glass properties and structure, particularly with respect to variation of the local site geometry, intertetrahedral angles, ring statistics and their relationship to chemical ordering, clustering and/or substitution. A fundamental question is to determine whether or not germanosilicate glasses form a homogeneous network or if there is some sort of clustering or phase separation.

5.1. EXAFS and x-ray scattering

An early Ge *K*-edge EXAFS investigation [99] on $12.5GeO_2$–$87.5SiO_2$ and $36.5GeO_2$–$63.5SiO_2$ glasses calculated a Ge–O distance of 1.73 ± 0.01 Å but no second neighbours were observed. A more extensive study using a combination of Ge *K*-edge x-ray absorption and wide-angle x-ray scattering (WAXS) experiments were carried out on GeO_2–SiO_2 glasses containing 16–36 mol% GeO_2 [100]. They showed that the XANES spectra are similar with increasing GeO_2 content and that EXAFS-derived distances are 1.72 ± 0.02 Å for Ge–O. A Ge coordination number of 3.9 ± 0.2, consistent with Ge in tetrahedral sites as in vitreous GeO_2, and a mean Si–O distance of 1.62 Å, consistent with Si remaining tetrahedrally coordinated, were obtained from their WAXS data. These results seem to be contradicted by a high-energy x-ray diffraction study on a $29GeO_2$–$71SiO_2$ composition glass [101] that found a mean coordination number for Si and Ge of 3.4 ± 0.05. The authors explain this low coordination number by proposing that a considerable number of Ge atoms are connected with fewer than four oxygens or are highly distorted. Except for the latter study, whose coordination number seems questionable, all structural studies are consistent with the presence of SiO_4 and GeO_4 tetrahedra in binary SiO_2–GeO_2 glasses.

The first peak observed in the x-ray radial distribution function is at higher distance than would be expected assuming standard Si–O and Ge–O distances (1.62 and 1.72 Å respectively for tetrahedral environment [100]). This suggests that the binary glasses are not a simple physical mixture of SiO_2 and GeO_2 oxides. In germanosilicate glasses, no GeO_2 clusters are observed and GeO_4 tetrahedra are thus part of the SiO_2 network. This is confirmed by the second shell of neighbours that has been observed in EXAFS data [100]. Indeed, this peak corresponds to Si and/or Ge neighbours and both its position and its intensity vary upon Si/Ge substitution. Ge atoms can thus be accommodated within the SiO_2 network. Intertetrahedral

angles were calculated from EXAFS and WAXS data and are between 139° and 149°, which is closer to 144° for SiO_2 glass (albeit the magnitude of this angle remains controversial, cf [102]) than 133° for GeO_2 glass. This suggests that at low GeO_2 content the Ge environment is constrained by the silicate network. These results are consistent with a substitutional model in which Ge substitutes randomly for Si in the vitreous SiO_2 network with little Ge clustering. A random substitution model is further supported by recent ^{17}O multiple quantum NMR spectra on GeO_2–SiO_2 binary glasses, which show peaks for all three types of bridging oxygens (Ge–O–Ge, Ge–O–Si, Si–O–Si), in proportions at least roughly consistent with random mixing of the tetrahedral cations [103].

The binary SiO_2–GeO_2 glass structure can be described by a continuous random network of corner sharing GeO_4 and SiO_4 tetrahedra.

5.2. Raman spectroscopy

Information on the medium-range structure such as ring statistics and the ordering of Si and Ge atoms has been primarily obtained by Raman spectroscopic investigations of germanosilicate glasses. Important modifications appear between the Raman spectra of pure GeO_2 and SiO_2 and some specific structures are present in the spectra of the binary glasses.

The band at low frequency shifts from 437 cm^{-1} in SiO_2 to 416 cm^{-1} in GeO_2 and becomes sharper [104]. This band is attributed to the T–O–T (T = Si or Ge) symmetric stretching mode and is thus characteristic of the distribution maximum in the T–O–T intertetrahedral angles [105]. Therefore, it can be concluded that the fluctuation in the intertetrahedral angle decreases as GeO_2 is introduced into the silica network.

A complete Raman study from pure SiO_2 to pure GeO_2 was carried out by Sharma *et al* [104] in order to characterize the distribution of SiO_4 and GeO_4 tetrahedra. In the germanosilicate glasses, a weak band in the range 970–1010 cm^{-1} appears that is not present in pure SiO_2 or GeO_2 glasses. This band is attributed to the antisymmetric stretching motion of the bridging oxygen of Si–O–Ge linkages, while the corresponding modes for the Si–O–Si and Ge–O–Ge linkages appear at $\simeq$1110 cm^{-1} and $\simeq$880 cm^{-1}, respectively. The position of the band is at $\simeq$1000 cm^{-1} for the $10GeO_2$–$90SiO_2$ glass but decreases to $\simeq$920 cm^{-1} for the $90GeO_2$–$10SiO_2$ glass. This shift in position towards lower frequency is attributed to a decrease in the Si–O–Ge bond angle in the GeO_2-rich glasses [104]. In the $50GeO_2$–$50SiO_2$ glass, the bands at 1100 and 880 cm^{-1} are stronger than the one at 980 cm^{-1}. This indicates the formation of Si–O–Ge bonds but also the existence of an important number of Si–O–Si and Ge–O–Ge linkages. According to these authors, the Si/Ge ordering is likely non-ideal, which supports a random distribution of SiO_4 and GeO_4 tetrahedra (see comment above regarding ^{17}O NMR). In a molecular dynamics simulation of a $50GeO_2$–$50SiO_2$ glass [106], a large fraction of Ge–O–Si bonds were found, as well as Ge–O–Ge and Si–O–Si linkages. Based on the simulations, Bernard *et al* [106] proposed that Ge/Si ordering occurred but not to the extent that phase separation was evident. They also showed that non-bridging oxygens (5%) were mainly localized in the Ge environment.

With a small addition of GeO_2, the D_1 and D_2 lines of SiO_2 glass at 495 and 606 cm^{-1}, attributed to four-membered and three-membered rings of the SiO_4 tetrahedra in vitreous silica, are still observed, but the intensity of the D_1 line decreases sharply, while that of the D_2 lines decreases slowly and broadens [107]. Nian *et al* [107] suggested that the substitution of Ge for Si in the vitreous SiO_2 network prevents the formation of these ring structures. This was explained by the disruption of the fourfold and threefold SiO_4 rings to accommodate the larger GeO_4 tetrahedra that distort the silicate network. Alternatively, the decrease in intensity of D_1 and D_2 lines could also be due to a change in polarizability of the Si–O bonds as Ge pulls

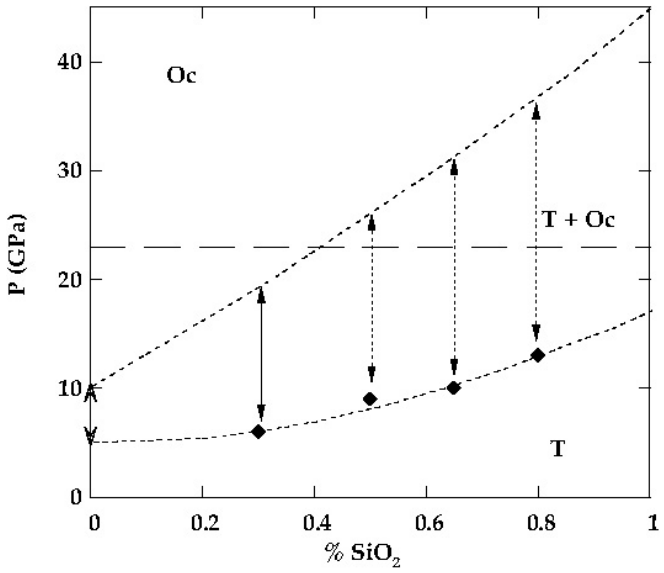

Figure 9. Pressure–composition diagram of the SiO_2–GeO_2 glasses (after [108]), depicting the pressure-induced Ge coordination change. The horizontal dashed line separates the pressure range explored. Diamonds are the pressure onsets of the coordination change and the dashed curves delimit the intermediate domain separating the low-density form (T for tetrahedral) and high-density form (Oc for octahedral).

electron density away from O attached to Si, which is an explanation more consistent with the preference for three-membered rings in GeO_2 relative to SiO_2 as indicated by diffraction and Raman data (see above). With small addition of GeO_2, a new band appears at 710 cm^{-1} but its assignment is not clear [107]. Above 15 mol% GeO_2 content, weak and broad shoulders are exhibited at $\simeq$568 and $\simeq$670 cm^{-1} and the band at $\simeq$800 cm^{-1} decreases in intensity [104].

5.3. Evolution with pressure

The Ge coordination change in the tetrahedral framework SiO_2–GeO_2 glasses is a reversible process that has to been studied by *in situ* high-pressure XAS measurements at the Ge *K* edge [108]. The pressure–composition diagram in figure 9 shows the existence of three regions with distinct short-range structures. At low pressure, the region corresponds to a tetrahedral framework structure (T domain), then an intermediate domain with a mixture of different sites, while, at higher pressure, the Oc region corresponds to a structure with $^{[6]}$Ge. The $^{[4]}$Ge to $^{[6]}$Ge transformation is reversible with an important hysteresis (a return back to the tetrahedral site below 4 GPa). The coordination change is dependent on the mean composition of the glasses and extends over higher pressure range when the SiO_2 content increases. The remarkable dependence of the Ge coordination change on the SiO_2 content shows that the Ge local structure is strongly affected by Si. The disruption of the SiO_2 tetrahedral network begins at 10 GPa, as evaluated by Raman spectroscopy [85], which is similar to the XAS data at high SiO_2 content and indicates that Ge and Si convert to a sixfold coordination state simultaneously. This result suggests that the pressure-induced transformations occur homogeneously in the mixed network and may be driven by the oxygen atoms rather than by the Ge or Si atoms [85]. Indeed, in such fully polymerized networks, oxygens increase their coordination from two to three in the transformation. The transformation occurs at higher pressure and over a broader

pressure range when the SiO_2 content increases. A careful analysis of both XANES and EXAFS signals supports a model of a mixing of $^{[4]}$Ge and $^{[6]}$Ge states in the transition region, in agreement with a kinetically hindered first-order process for the transformation at room temperature.

6. Molecular simulations and theoretical approaches

6.1. Force field parameters

Several force field potentials have been proposed to describe either the crystalline phases of GeO_2 or amorphous germania. All these potentials contain a long-range Coulombic part, along with a short-range repulsive term and an additional van der Waals-like term

$$V_{ij}(r_{ij}) = \frac{Z_i Z_j e^2}{r_{ij}} + A_{ij}\mathrm{e}^{-r_{ij}/\rho_{ij}} - \frac{C_{ij}}{r_{ij}^6} \tag{1}$$

where Z_i is the charge on ion i. The parameter ρ_{ij} serve to determine the steepness of the short-range repulsive potential and is known as the '*softness*' parameter. The parameters A_{ij} and C_{ij} serve to adjust the positions of the first peak in each possible radial distribution function to experimental findings. Oeffner and Elliot [109] have fitted equation (1) to obtain cell parameters, density and elastic constants of the trigonal α-quartz-like and tetragonal rutile-like phases of GeO_2. Bond angles and bond lengths in both the low- and high-pressure phases are found to agree with experimental findings. The Raman and infrared vibrational spectra are also simulated within the harmonic approximation using the bond-polarizability model of Long [110]. Analysis from the vibrational density of states of Ge–O–Ge motions shows that for α-quartz-like GeO_2 symmetric and asymmetric bending motions are mostly confined to medium- and low-frequency bands, while symmetric stretching and bending motions can be reasonably simulated at the anticipated frequencies.

Matsui and co-workers [111] have used the same kind of approach, i.e. the fitting of equation (1), to simulate another structural phase transition, namely the pressure-induced change from α-quartz-like GeO_2 to rutile-like GeO_2, which happens at 7.4 GPa. The structure obtained at this pressure appears to be quite similar to the structure calculated for SiO_2 at 21.5 GPa [112]. Furthermore, it is shown that α-quartz-like GeO_2 close to the transition is mechanically unstable as some of the elastic moduli of the lattice become negative. Specifically, the decrease of the transverse elastic constant C_{44} leads to an unstable shear that originates the transformation to the rutile-like structure. For increased pressures, a post-rutile-like structure is found [11] that has a $CaCl_2$-like structure which consists of tilted GeO_6 octahedra. This appears to be in agreement with Brillouin scattering results of α-GeO_2 under pressure [113], which show that the shear constants are largely softened with respect to SiO_2 and can be related to shear instability.

More recently, an alternative model has been proposed by Van Hoang [114] for liquid and amorphous germania that is based on a Morse-like potential in a similar manner to the potential given by Kim for GeO_2 [115]. We discuss below the structural predictions of the Van Hoang potential. For completeness, we mention also the model potential proposed by Nanba [116] to account for GeO_2–PbO–PbF_2 glasses. However, it appears to show poor agreement with the rutile-like properties of GeO_2.

Topological and geometrical approaches have also been proposed [117] in order to generate continuous random network models of GeO_2 that reproduce the experimental density, bond angle distributions and neutron scattering data [35]. Araujo has used statistical mechanical techniques [118] to calculate the density of oxygen vacancies in GeO_2 and the absorption coefficient with respect to temperature.

6.2. Simulation of liquid and amorphous germania

Most of the work using the effective potentials described above has been devoted to the description of the high-temperature liquid where experimental data are lacking. Gutierrez and Rogan [119] have simulated GeO_2 at 1500 and 3000 K. At these temperatures, the system seems to be made of slightly distorted GeO_4 tetrahedra which are linked by corners and have a Ge–O–Ge angle of 130°, similar to the experimental value in the amorphous phase (GeO_2 glass). A volume collapse, in the range 4–8 GPa, is seen from the pressure–volume curve and may be the signature of a liquid–liquid phase transition, in analogy with water [120]. Van Hoang has carried out a similar study [121] under the same kind of conditions, i.e. in the high-temperature (5000 K) liquid with changing density, and has suggested that a diffusion maximum should be attained for a density of about 5 g cm^{-3}. This anomaly appears to be produced by competition between the breakdown of the tetrahedral network structure, leading to an increase in atomic mobility, and the packing effects arising from densification that tend to reduce the mobility. The simulated structure of liquid GeO_2 and SiO_2 appears to be very similar when the partial atomic correlation functions are properly rescaled [122].

Micoulaut *et al* [59] have used the Oeffner–Elliot potential to study the glass and liquid phases, which allows comparison with experiments. In the glass, the structural properties can be simulated relatively well, even though some structural limitations of the potential appear. While the first structural peak due to Ge–O interactions can be modelled very well at the expected distance of 1.72 Å, as can the O–O distance at 2.81 Å, the Ge–Ge correlations appear to be slightly overestimated (3.32 Å) with respect to experimental values. This overestimation leads to a larger calculated value for the intertetrahedral angle than that obtained experimentally: 159° versus 130°, respectively. It is now well known that simple ionic potentials such as the ones reported above [109, 11] result in Ge–O–Ge angles that are too wide, a situation that has been encountered and reported already for amorphous silica [123]. However, the absence of any Ge–Ge interaction in the effective Oeffner–Elliot potential, except in the Coulombic term, may be responsible for the increased distortion in germania with respect to silica. In spite of these deficiencies, the simulation correctly describes the structure factor $S(Q)$ and the partial structure factors $S_{ij}(Q)$ (figure 5) and allows one to infer the origin of the first sharp diffraction peak (FSDP) as mostly arising from Ge–Ge correlations. However, overall the potential is found to reproduce the features of neutron scattering functions (figure 10) reported by different groups [35, 57].

Simulation using a Morse-like potential [114] provides a somewhat better agreement with the experimental partial atomic correlation functions (figure 10) as the Ge–Ge distance is found to be 3.21 Å at 300 K with correct bond angles ($\theta_{O–Ge–O} = 108°$ and $\theta_{Ge–O–Ge} = 133°$) whereas both Ge–O and O–O distances are slightly underestimated (1.69 and 2.78 Å respectively) relative to experimentally derived values.

6.3. Glass transition problem of strong glasses

Enthalpy and glass transition temperature can be simulated rather well [59] with respect to calorimetric measurements [124]. With the Oeffner–Elliot potential, a T_g of 900 K is found from the inflexion point of the potential energy. This value is close to the experimental derived T_g (850 K, [125]). This appears to be rather unusual, as MD simulations on similar systems [126, 127] predict much higher glass transition temperatures than the corresponding experimental ones. This is partially due to the high quench rates applied. In the present simulated systems, onset of slow dynamics at the nanosecond scale occurs in the same range of temperatures (920 K) which corroborate the calculated T_g from the inflexion point of the energy profile.

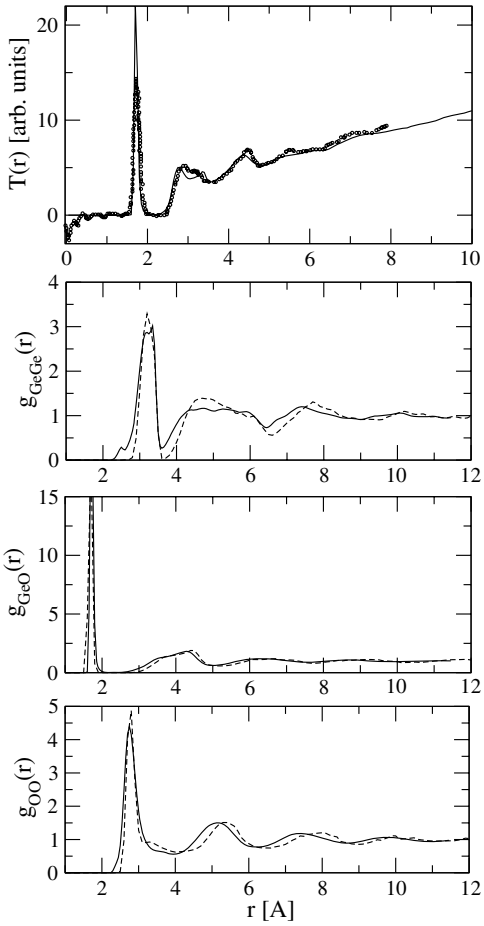

Figure 10. Upper panel: simulated (dashed) neutron structure [59] factor $T(r)$ compared to experimental findings [57]. Lower panels: partial structure factors of 300 K amorphous GeO_2 using the Oeffner–Elliot (solid line) [109] and the Morse-like potential (broken line) [114].

When put in contrast with silica, a more careful inspection of the self-diffusion coefficient D with respect to the viscosity behaviour [128] shows that the agreement between the simulated and experimentally measured T_g reveals an underlying failure of the simulation technique. The self-diffusion coefficient D is computed from the mean-squared displacement of the germanium and oxygen atoms, and shows Arrhenius-like behaviour $D = D_0 \exp[E_i/T]$ at low temperatures, whereas at higher temperatures ($T > 1600$ K) some curvature appears (figure 11), similar to that found for molten silica [129]. However, the calculated oxygen diffusion constant for GeO_2 at 1440 K is several orders of magnitude larger than the reported data for oxygen diffusion ($D_O = 7 \times 10^{-14}$ m^2 s^{-1}, [130]). A predicted diffusion constant D from viscosity data η using the Eyring relation $k_B T/\eta D = \lambda$ (where λ is a hopping length of about several ångströms [131]) shows that both silica and germania overestimate the diffusion constants with respect to their simulated T_g values, thus allowing the system to remain in a liquid-like behaviour to lower temperatures. This underscores both the limitation of the employed potentials and the size of the simulated systems (actually up to several thousand atoms) to accurately describe the glass transition of strong glass formers.

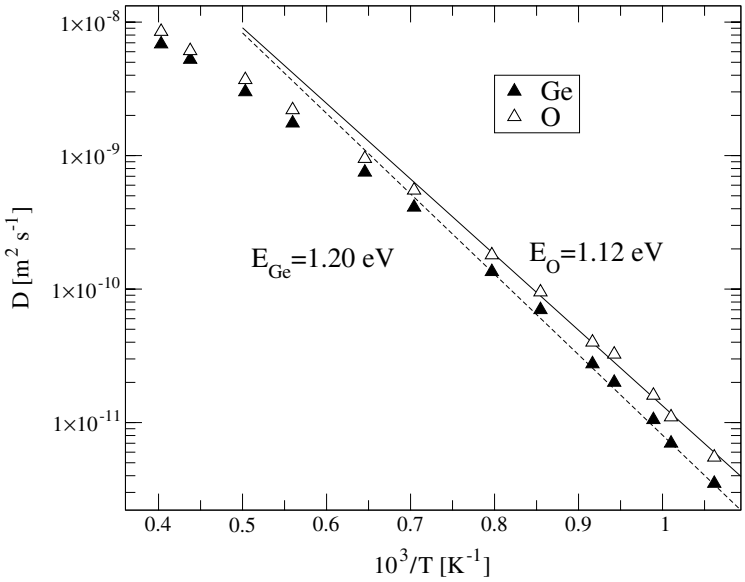

Figure 11. Simulated diffusion for germanium and oxygen using the Oeffner–Elliot potential [59].

6.4. Equation of state

The equation of state (EOS) of GeO_2 has been reported by different authors, either on the basis of simulations [119] or from empirical models based on simple structural arguments [132]. In the latter, Smith and co-workers have shown that a two-state function, taking into account the effect of the tetrahedral and octahedral character at low and high pressures, is able to describe the experimental equation of state at 300 K, whereas molecular dynamics simulations only succeed in simulating the EOS in the low pressure range.

At higher temperatures and higher densities, Gutierrez and Rogan [119] have shown that for simulated GeO_2 in the 3.5–5.6 g cm^{-3} and $T = 1500$–3000 K range, pressure displays a monotonic decrease with molar volume. In the same context, a Birch–Murnaghan type [133] of EOS has been used [59] to fit a set of 269 simulated state points in the thermodynamic diagram. The method allows the extraction of the isothermal compressibility κ_T as a function of temperature and density for density ranges lying between the ordinary glass density at 300 K ($\rho = 3.66$ g cm^{-3}, [67]) and about 2.5 g cm^{-3}. Progressive deviation of the Birch–Murnaghan EOS with respect to the simulated thermodynamic points appear for $\rho < 2.5$ g cm^{-3} at high temperatures. At 2000 K, the computed compressibility ($\kappa_T = 9.13 \times 10^{-11}$ Pa^{-1}) is rather close to the experimentally measured value of Dingwell *et al* ($\kappa_T = 12.4 \times 10^{-11}$ Pa^{-1}, [134]).

Micoulaut and Guissani [59] have used a direct molecular dynamics method [135] to follow the equation of state at zero pressure, in order to predict the liquid–vapour coexistence curve of germania on the low- (vapour) and high-density (liquid) side in order to compare it with experimental results in the liquid up to 1440 K [67]. Furthermore, the method highlights the quality of the effective potentials employed at low temperature. At zero pressure and low temperature (300 K), the density of a simulated Oeffner–Elliot GeO_2 glass [109] is indeed 3.70 g cm^{-3}, whereas the density of a simulated GeO_2 glass using an alternative potential [11] substantially disagrees with the experimental low-temperature density of the liquid ($\rho = 4.25$ g cm^{-3} as compared to the experimental $\rho = 3.66$ g cm^{-3}). Note however that this potential was used to study pressure-induced rigidity in GeO_2 (see below, [136])

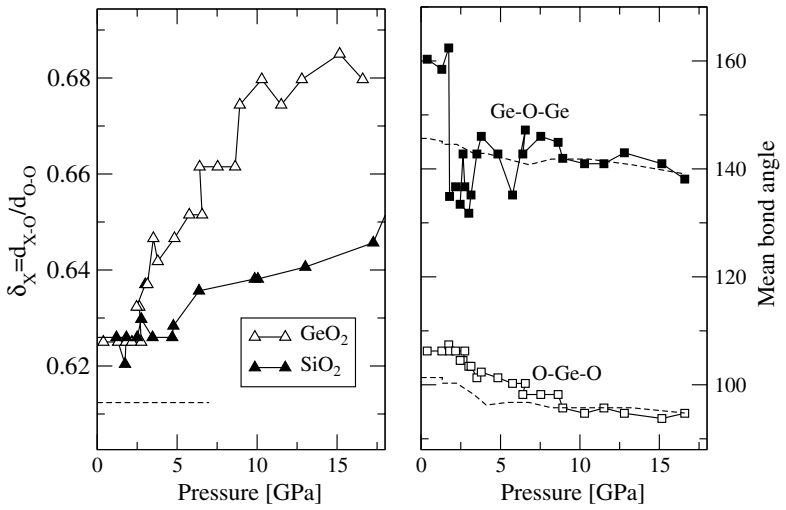

Figure 12. Local structure of germania with applied pressure [60]. Left panel: distortion parameter δ_X of regular GeO_4 and SiO_4 tetrahedra, as a function of applied pressure (X = Ge, open triangles). For comparison, the same parameter for SiO_2 (X = Si, filled triangles) is shown. The broken horizontal line represents the value of the perfect tetrahedron $\delta = \sqrt{3/8}$. Right panel: mean bond angles Ge–O–Ge and O–Ge–O with respect to compression (open and filled symbols) and decompression (broken curves).

and the density at zero pressure was found [137] to be 3.9 g cm^{-3}, i.e. much closer to the experimental value. The thermal history of the simulation appears therefore to be crucial in this case.

Using a Wegner type expansion [138], a critical point for germania is predicted and is located at $T_c = 3658$ K, $\rho_c = 0.59$ g cm^{-3} and $P_c = 40$ MPa [139]. For the Tsuchiya potential [11], the location of the critical point seems to be much higher in temperature [140]. This shift may arise from the increased charges used in the effective potential.

6.5. Pressurized germania

The application of pressure to amorphous germania seems to affect the structure stepwise. Experimentally, a jump in bond distance from 1.72 to 1.86 Å is observed at around 9 GPa, signalling the conversion of tetrahedral to octahedral local structure as already described. However, numerical simulations show [60], at least in the low pressure range, that this conversion is somewhat more subtle. For pressures up to 2 GPa, long-range correlations are reduced, as seen from the shift to higher wavevector of the position of the FSDP, similar to experimental observations [141]. In addition, a reduction is observed in the intertetrahedral bond angle (Ge–O–Ge) and then for $P = 3$ GPa a sharp distortion of the GeO_4 tetrahedron occurs (figure 12). These results are accompanied by a global increase in the number of oxygen neighbours in the vicinity of a germanium atom that parallel the increase in density [59].

Sharma and co-workers [142] have studied both the pressure-induced structural changes of the α-quartz-like GeO_2 polymorph and amorphous GeO_2 using the Oeffner–Elliott potential in the (N, P, T) ensemble. The results show that both the average bond distance (Ge–O) and the average Ge coordination in α-quartz-like GeO_2 undergo a sharp change at around 8 GPa under compression, similar to the experimental findings of Itié *et al* [8]. On decompression, the denser phase transforms back to a lower-density phase at $\simeq$2 GPa. The details of the number of oxygen neighbours around a Ge atom show, however, that the high-density phase is not

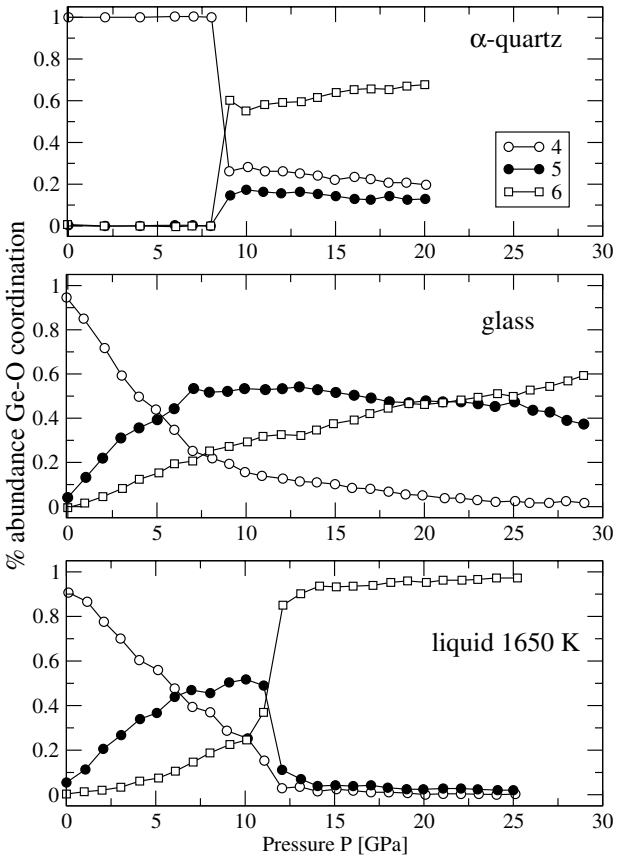

Figure 13. Calculated variation with pressure [142] of the fractional abundance of Ge coordination in the α-quartz-like GeO_2 polymorph, glassy (300 K) and liquid GeO_2 (1650 K).

fully sixfold coordinated, as about 15% fivefold and 20% fourfold germanium can be found (figure 13). Less abrupt changes are expected for vitreous GeO_2 (figure 13), where a majority of sixfold germanium only occurs for pressures larger than 20 GPa.

The structural changes with pressure are more dramatic in liquid (1650 K) GeO_2 as a sudden loss of fivefold germanium atoms and an almost sixfold coordinated structure is obtained for pressures larger than 12 GPa.

Finally, it appears that the evolution of the intermediate-range order with pressure or density is selective as MD simulated ring statistics [143] show that rings with more than six germania tetrahedra tend to disappear for densities larger than 5 g cm^{-3}, whereas the growth of edge-sharing GeO_6 octahedra signals a behaviour similar to TiO_2.

6.6. Pressure-induced rigidity and intermediate phases

Trachenko *et al* [144, 145] have been investigating the network rigidity of GeO_2 and SiO_2 under pressure. Rigidity usually appears when the number of mechanical constraints per atom, arising from interatomic interaction (mostly bond stretching and bond bending), becomes greater than the number of degrees of freedom [146]. In network glasses, this is generally achieved by the addition of cross-linking elements such as germanium into a basic flexible structure containing

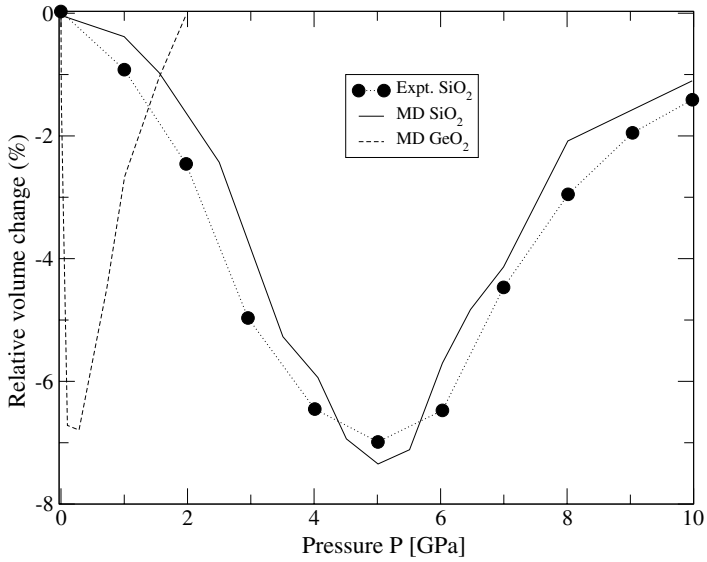

Figure 14. Relative variation in volume in GeO_2 and SiO_2 glasses under pressure compared with experiments on SiO_2 [136].

e.g. selenium chains. This leads to an increase of the network mean coordination number $\bar{r}$ (and to the increase of constraints) and produces a stiffening of the structure and ultimately a floppy to rigid transition. The onset of rigidity and the way it percolates has been documented for various glass-forming systems. In recent years, however, a reversibility window [147, 148] has been discovered located between the floppy and rigid phases, which manifests itself by the loss of irreversibility (and hysteresis) of the heat flow when cycling through the glass transition temperature region. A similar state can be found in glassy GeO_2 and SiO_2 under pressure.

Pressure-induced rigidity in GeO_2 glass using MD simulations has been addressed recently [136]. Here the increase in connectivity (or mean coordination number $\bar{r}$) is achieved with the increase of the glass density or the application of pressure that produces a tetrahedral to octahedral conversion. Thus pressure introduces locally rigid higher-coordinated units in an otherwise flexible tetrahedral network of GeO_4 tetrahedra. Densification with temperature under pressure can take place in a pressure window, centred around the rigidity percolation transition. The density change is about 7%. This new effect has been rather well documented for silica [144, 145] and compared successfully with experimental results [149] and additional simulations showing the loss of low-frequency modes in the effective vibrational densities of states at the same pressure where densification occurs. However, it has only been shown that the pressure window in germania is centred around 0.5 GPa, i.e. considerably lower than for silica (5 GPa) (figure 14). However, it is another signature of the increased sensitivity to pressure change of GeO_2 with respect to SiO_2. Indeed, the tetrahedral to octahedral conversion of amorphous SiO_2 manifested by the jump in Si–O bond distances is found to be around 13 GPa [150], whereas the same jump is found to be at 8 GPa for GeO_2 glass [8]. It is therefore not surprising at all that onset of rigidity manifests at lower pressures in GeO_2.

6.7. Ab initio studies of c-GeO_2 and germania

One way to circumvent the possible failures of the above mentioned semi-empirical potentials is the use of *ab initio* methods, especially under extreme conditions where the potentials are not

necessarily reliable. Hafner and co-workers [19] have studied the high-pressure transformations up to 70 GPa of crystalline GeO_2, using density functional theory with a pseudopotential method, and a local density approximation. It appears from this computation that several high-pressure phases can exist in GeO_2, which are a tetragonal $CaCl_2$ type at 40 GPa, an α-PbO_2-type at 40 GPa and finally a pyrite-type crystal at 70 GPa, similar to those observed experimentally (see above) (figure 3). These transformations highlight the analogy of the phase transition sequence between SiO_2 and GeO_2 polymorphs at high pressure. Additional studies concerning the electronic properties of these polymorphs have been reported by Christie *et al* [151], using the same tools. This allows determination of the lattice parameters, cohesive energy and bulk modulus by minimizing the total energy of the solid. In addition, an equation of state for the polymorphs can be fitted with a Birch–Murnaghan EOS [133, 152] or the density of states.

Ab initio studies of amorphous germania have been only reported recently [58] using the same numerical scheme but with an improved density approximation (generalized gradient). This enables determination of the neutron structure factor (figure 4), the infrared and the Raman spectra, all of which show good agreement with experimentally derived data (cf, figure 8(c)). It furthermore provides insight into the three-membered ring distribution and the so-called D_2 line first described by Galeener and workers [82]. The projection of vibrational eigenmodes onto natural or isotopic substituted oxygen breathing motions in these rings shows that a broad peak centred at 520 cm^{-1} and corresponding to the experiment is blueshifted with ^{18}O by 26 cm^{-1}. The number of these rings is found to be about 20% of the oxygen atoms. On the other hand, similar calculations do not seem to support the assignment of four-membered rings to the D_1 line found at 347 cm^{-1}. Instead, this band seems to arise from coupled motions of Ge and O atoms.

7. Summary and conclusions

Studies on the structure of crystalline, liquid and glassy GeO_2 continue to be of interest to a number of researchers in physics and glass, materials and geological sciences. This breadth of interest stems from the fact that while there are close similarities between GeO_2 and SiO_2 there are also distinct differences, which make GeO_2 useful as an analogue for studying the high-pressure behaviour of oxide glasses. Crystalline GeO_2 polymorphs behave, with increasing temperature and pressure, in a manner similar to crystalline SiO_2 polymorphs. However, pressure-induced phase transformations generally occur at much lower pressures than equivalent SiO_2 phases. This is because the larger GeO_4 tetrahedron (relative to the SiO_4 tetrahedron) is more distorted due to greater variability in the O–Ge–O angles. This makes the use of GeO_2 polymorphs attractive as SiO_2 analogues in high-pressure studies for studying possible pressure-induced structural changes, since the pressure ranges required are much more accessible.

GeO_2 glass has also been considered as being somewhat similar to SiO_2 glass. The first three interatomic distances in the glass are reasonably well resolved and indicate that, like SiO_2 glass, the network is composed of tetrahedra linked together through their corner bridging oxygens. However, there are significant differences between the two glass networks. GeO_2 glass has a much smaller mean Ge–O–Ge angle and a much higher proportion of three-membered rings, relative to SiO_2 glass. Furthermore, there may be differences in the intermediate-range structure, with GeO_2 glass possibly being composed of four-membered rings, rather than the currently accepted six-membered rings similar to SiO_2 glass. In addition, application of high pressure readily converts fourfold Ge to sixfold Ge, via a transitional fivefold coordination, at much lower pressures than found for SiO_2 glass. In the liquid state GeO_2 retains fourfold geometry to high temperature but with broadened Ge–O–Ge angles,

although numerical studies of liquid GeO_2 indicate that while the GeO_4 tetrahedra are distorted the Ge–O–Ge angle remains similar to that found in the α-quartz-like GeO_2 polymorph. Furthermore, simulation of pressure effects indicates that the pressure-induced transformation from four- to sixfold Ge observed experimentally at $\simeq$9 GPa may be quite subtle. Onset of the simulated transition occurs at 2 GPa with loss of long-range correlations, a reduction in the Ge–O–Ge angle, followed by a sharp distortion of the GeO_4 tetrahedra at 3 GPa. This is accompanied by the onset of rigidity at much lower pressure than observed for SiO_2 glass. When Ge substitutes for Si along the GeO_2–SiO_2 binary, there is no evidence for clustering or phase separation of the glass network and it is composed of SiO_4 and GeO_4 tetrahedra. The substitution is random, with no heterogeneity induced in the combined network. However, with increasing pressure Ge undergoes a coordination change from four- to sixfold coordination. The pressure at which this occurs is dependent upon the SiO_2 composition, indicating that Si has an influence on the local structure of Ge. In addition, there is a broad pressure–composition range over which Ge is in both four- and sixfold coordination.

Acknowledgments

GSH acknowledges funding from NSERC via a Discovery grant. He also thanks his co-authors, the Institut de Minéralogie et Physique des Milieux Condensés (IMPMC) and the CNRS for a very enjoyable stay at IMPMC. The authors acknowledge discussions and correspondence with P Boolchand, G Calas, M T Dove, S R Elliott, G Ferlat, L Giacomazzi, B Guillot, Y Guissani, G Hovis, A Pasquarello, J C Phillips, D L Price, P Richet, J F Stebbins and K Trachenko.

References

[1] Zachariasen W H XIII 1928 Uber die Kristallstruktur der wasserl?chen Modifikation des Germaniumdioxyd *Z. Kristallogr.* **67** 226–34
[2] Smith G S and Isaacs P B 1964 The crystal structure of quartz-like GeO_2 *Acta Crystallogr.* **17** 842–6
[3] Baur W H and Khan A A 1971 Rutile-type compounds. IV. SiO_2, GeO_2 and a comparison with other rutile-type structure *Acta Crystallogr.* B **27** 2133–9
[4] Laubengayer A W and Morton D S 1932 Germanium. XXXIX. The polymorphism of germanium dioxide *J. Am. Ceram. Soc.* **54** 2302–20
[5] Jorensen J D 1978 Compression mechanisms in α-quartz structures—SiO_2 and GeO_2 *J. Appl. Phys.* **49** 5473–8
[6] Ault K M and Secco R A 1996 High pressure conductivity study of the α quartz-rutile transformation in GeO_2 *Solid State Commun.* **98** 449–52
[7] Yamanaka T, Sugiyama K and Ogata K 1992 Kinetic study of the GeO_2 transition under high pressure using synchrotron x-radiation *J. Appl. Crystallogr.* **25** 11–5
[8] Itie J P, Polian A, Calas G, Petiau J, Fontaine A and Tolentino H 1989 Pressure-induced coordination changes in crystalline and vitreous GeO_2 *Phys. Rev. Lett.* **63** 398–401
[9] Wolf G H, Wang S, Herbst C A, Durben D J, Oliver W F, Kang Z C and Halvorson K 1992 Pressure induced collapse of the tetrahedral framework in crystalline and amorphous GeO_2 *High Pressure Research: Applications to Earth and Planetary Sciences* (Tokyo: Terra Scientific)
[10] Kawasaki S, Ohtaka O and Yamanaka Y 1994 Structural change of GeO_2 under pressure *Phys. Chem. Minerals* **20** 531–5
[11] Tsuchiya T, Yamanaka T and Matsui M 1998 Molecular dynamics study of the crystal structure and phase relation of the GeO_2 polymorphs *Phys. Chem. Minerals* **25** 98–100
[12] Brazhkin V V, Tat'yanin E V, Lyapin A G, Popova Tsiok O B and Balitskii D V 2000 Technology of high pressure *Proc. Int. Conf. on High Pressure Science and Technology* ed M H Manghnani, W J Ellis and M F Nicol (Hyderabad: University Press)
[13] Brazhkin V V, Tat'yanin E V, Lyapin A G, Popova Tsiok O B, Balitskii D V and Pis'ma Zh 2000 Martensitic transition in single-crystalline α-GeO_2 at compression *JETP Lett.* **71** 293–7

[14] Brazhkin V V, Lyapin A G, Voloshin R N, Popova S V, Tat'yanin E V, Borovikov N F, Bayliss S C and Sapelkin A V 2003 Pressure-induced cross-over between diffusive and displacive mechanisms of phase transitions in single-crystalline a-GeO_2 *Phys. Rev. Lett.* **90** 145503

[15] Haines J, Leger J M and Chateau C 2000 Transition to a crystalline high-pressure phase in α-GeO_2 at room temperature *Phys. Rev.* B **61** 8701–6

[16] Prakapenka V B, Dubrovinsky L S, Shen G, Rivers M L, Sutton S R, Dimitriev V, Weber H-P and Le Bihan T 2003 α-PbO_2-type high-pressure polymorph of GeO_2 *Phys. Rev.* B **67** 132101

[17] Haines J, Leger J M, Chateau C and Periera A S 2000 Structural evolution of rutile-type and $CaCl_2$ type germanium dioxide at high pressure *Phys. Chem. Minerals* **27** 575–82

[18] Ono S, Hirose K, Nishiyama N and Isshiki M 2002 Phase boundary between rutile-type and $CaCl_2$-type germanium dioxide determined by *in situ* x-ray observations *Am. Mineral.* **87** 99–102

[19] Lodziana Z, Parlinski K and Hafner J 2001 *Ab initio* studies of high-pressure transformations in GeO_2 *Phys. Rev.* B **63** 134106

[20] Ono S, Tsuchiya T, Hirose K and Ohishi Y 2003 Phase transition between the $CaCl_2$-type and a α-PbO_2-type structures of germanium dioxide *Phys. Rev.* B **68** 014103

[21] Ono S, Tsuchiya T, Hirose K and Ohishi Y 2003 High-pressure form of pyrite-type germanium dioxide *Phys. Rev.* B **68** 014103

[22] Bassett L-G, Liu W A and Sharry J 1978 New high pressure modifications of GeO_2 and SiO_2 *J. Geophys. Res.* **83** 2301–5

[23] Prakapenka V B, Shen G, Dubrovinsky L S, Rivers M L and Sutton S R 2004 High pressure induced phase transformations of SiO_2 and GeO_2: difference and similarity *J. Phys. Chem. Solids* **65** 1537–45

[24] Shiraki K, Tsuchiya T and Ono S 2003 Structural refinement of high-pressure phases in germanium dioxide *Acta Crystallogr.* B **59** 701–8

[25] Ming L C and Manghnani M H 1983 High-prssure phase transformation in vitreous and crystalline GeO_2 (rutile) *Phys. Earth Planet. Inter.* **33** 26–30

[26] Teter D M, Hemley R J, Kresse G and Hafner J 1998 High pressure polymorphism in silica *Phys. Rev. Lett.* **80** 2145–8

[27] Yamanaka T and Ogata K 1991 Structure refinement of GeO_2 polymorphs at high pressure and temperatures by energy-dispersive spectra of powder diffraction *J. Appl. Crystallogr.* **24** 111–8

[28] Glinnemann J, King H E Jr, Schulz H, Han Th, La Placa S J and Dacol F 1992 Crystal structures of the low-temperature quartz-type phases of SiO_2 and GeO_2 at elevated pressure *Z. Kristallogr.* **198** 177–212

[29] Haines J, Cambon O, Philippot E, Chapon L and Hull S 2002 A neutron diffraction study of the thermal stability of the α-quartz-type structure in germanium dioxide *J. Solid State Chem.* **166** 434–41

[30] Balitsky D V, Balitsky V S, Pisarevsky Yu V, Philippot E, Silvestrova O Yu and Pushcharovsky D Yu 2001 Growth of germanium dioxide single crystals with α-quartz structure and investigation of their crystal structure, optical, elastic, piezoelectric, dielectric and mechanical properties *Ann. Chim. Sci. Mater.* **26** 183–92

[31] Madon M, Gillet Ph, Julien Ch and Price D G 1991 A vibrational study of phase transitions among the GeO_2 polymorphs *Phys. Chem. Minerals* **18** 7–18

[32] Bohm H 1968 The cristobalite modification of GeO_2 *Naturwissenschaften* **55** 648–9

[33] Hauser E, Nowotny H and Seifert K J 1970 Uber die GeO_2-modifikationen (zerfall) des ammonium-hydrogermanates *Monatsh. Chem.* **101** 715–20

[34] Leadbetter A J and Wright A C 1972 Diffraction studies of glass structure II. The structure of vitreous germania *J. Non-Cryst. Solids* **7** 37–52

[35] Desa J A E, Wright A C and Sinclair R 1988 A neutron diffraction investigation of the structure of vitreous germania *J. Non-Cryst. Solids* **99** 276–88

[36] Sarver J F and Hummel F A 1960 Alpha to beta transition in germania quartz and a pressure temperature diagram for GeO_2 *J. Am. Ceram. Soc.* **43** 336

[37] Warren B E 1934 The diffraction of x-rays in glass *Phys. Rev.* **45** 657–61

[38] Warren B E 1934 X-ray determination of the structure of glass *J. Am. Ceram. Soc.* **17** 249–54

[39] Zarzycki J 1956 Etude du réseau vitreux par diffraction des rayons X aux temperatures elevees, travaux IV *Congres Int. du Verre (Paris)* pp 323–30

[40] Zarzycki J 1957 Sur l'angle de la liaison Si–O–Si de la silice vitreuse et celui de la liaison Ge–O–Ge de l'oxyde de germanium vitreux ou liquide *Verres et Refractaires* **11** 3–8

[41] Lorch E 1969 Neutron diffraction by germania, silica and radiation-damaged silica glasses *J. Phys. C: Solid State Phys.* **2** 229–37

[42] Ferguson G A and Hass M 1970 Neutron diffraction investigation of vitreous germania *J. Am. Ceram. Soc.* **53** 109–11

[43] Sinclair R N, Johnson D A G, Dore J G, Clarke J H and Wright A C 1974 Structural studies of amorphous materials using a pulsed neutron source *Nucl. Instrum. Methods* **117** 445–54
[44] Sinclair R N and Wright A C 1977 Diffraction studies of glasses using the Harwell electron LINAC pulsed neutron source *The Physics of Non-crystalline Solids* (Aedermannsdorf: Trans Tech)
[45] Neuefeind J and Liss K-D 1996 Bond angle distribution in amorphous germania and silica *Ber. Bunsenges. Phys. Chem.* **100** 1341–9
[46] Galeener F L 1982 Planar rings in glasses *Solid State Commun.* **44** 1037–40
[47] Barrio R A, Galeener F L, Martinez E and Elliott R J 1993 Regular ring dynamics in AX_2 tetrahedral glasses *Phys. Rev.* B **48** 15672–89
[48] Bondot P 1974 Essai de séparation des distributions de paires dans GeO_2 vitreux partir de l'effet de diffusion anomale *Acta Crystallogr.* A **30** 470–1
[49] Bondot P 1974 Study of local order in vitreous germanium oxide *Phys. Status Solidi* a **22** 511–22
[50] Waseda Y, Sugiyama K, Matsubara E and Harada K 1990 Partial structure functions for GeO_2 glass determined by the anomalous x-ray scattering data coupled with neutron diffraction *Mater. Trans. JIM* **31** 421–4
[51] Price D L, Saboungi M-L and Barnes A C 1998 Structure of vitreous germania *Phys. Rev. Lett.* **81** 3207–10
[52] Barnes A C, Hamilton M A, Buchanan P and Saboungi M-L 1999 Combined x-ray and neutron diffraction from binary liquids and amorphous semiconductors *J. Non-Cryst. Solids* **250–252** 393–404
[53] Price D L, Ellsion A J G, Saboungi M-L, Hu R-Z, Egami T and Howells W S 1997 Short-, intermediate-, and extended-range order in rubidium germanate glasses *Phys. Rev.* B **55** 11249–55
[54] Bhatia A B and Thornton D E 1970 Structural aspects of the electrical resistivity of binary alloys *Phys. Rev.* B **2** 3004–12
[55] Salmon P S, Martin R A, Mason Ph E and Cuello G J 2005 Topological versus chemical ordering in network glasses at intermediate and extended length scales *Nature* **435** 75
[56] Salmon P S, Barnes A C, Martin R A and Cuello G J 2006 Glass fragility and atomic ordering on the intermediate and extended range *Phys. Rev. Lett.* **96** 235502
[57] Stone C E, Hannon A C, Ishirawa T, Kitamura N, Shirakawa Y, Sinclair R N, Umesaki N and Wright A C 2001 The structure of pressure-compacted vitreous germania *J. Non-Cryst. Solids* **293–295** 769–75
[58] Giacomazzi L, Umari P and Pasquarello A 2005 Medium range structural properties of vitreous germania obtained through first-principles analysis of vibrational spectra *Phys. Rev. Lett.* **95** 075505
[59] Micoulaut M, Guissani Y and Guillot B 2006 Simulated structural and thermal properties of glassy and liquid germania *Phys. Rev.* E **73** 031504
[60] Micoulaut M 2004 Structure of densified amorphous germanium dioxide *J. Phys.: Condens. Matter* **16** L131–8
[61] Konnert J H, Karle J and Ferguson G A 1973 Crystalline ordering in silica and germania glasses *Science* **179** 177–9
[62] Hoppe U, Kranold R, Weber H-J, Neuefeind J and Hannon A C 2000 The structure of potassium germanate glasses—a combined x-ray and neutron scattering study *J. Non-Cryst. Solids* **278** 99–114
[63] Sugai S and Onodera A 1996 Medium-range order in permanently densified SiO_2 and GeO_2 glass *Phys. Rev. Lett.* **77** 4210–3
[64] Hemley R J, Meade C and Mao H-K 1997 Comments on medium range order in permanently densified SiO_2 and GeO_2 glass *Phys. Rev. Lett.* **79** 1420
[65] Sampath S, Benmore C J, Lantzk K M, Neuefeind J, Leinenweber K, Price D L and Yarger J L 2003 Intermediate-range order in permanently densified GeO_2 glass *Phys. Rev. Lett.* **90** 115502
[66] Guthrie M, Tulk C A, Benmore C J, Xu J, Yarger J L, Flug D D, Tse J S, Mao H-K and Hemley R J 2004 Formation and structure of a dense octahedral glass *Phys. Rev. Lett.* **93** 115502
[67] Kamiya K, Yoko T, Itoh Y and Sakka S 1986 X-ray diffraction study of Na_2O–GeO_2 melts *J. Non-Cryst. Solids* **79** 285–94
[68] Scott J F 1970 Raman spectra of GeO_2 *Phys. Rev.* B **1** 3488–93
[69] Dultz W, Quilichini M, Scott J F and Lehman G 1975 Phonon spectra of quartz isomorphs *Phys. Rev.* B **11** 1648–53
[70] Sharma S K 1989 *Applications of Advanced Raman Spectroscopic Techniques in the Earth Sciences* (*Raman Spectroscopy: Sixty Years on, Vibrational Spectra and Structure* vol 17B) (Amsterdam: Elsevier Science)
[71] Mernagh T P and Liu L-G 1997 Temperature dependence of Raman spectra of the quartz and rutile-types of GeO_2 *Phys. Chem. Minerals* **24** 7–16
[72] Bobovich Y S and Tolub T P 1958 Raman spectra of alkali-germanate glasses *Opt. Spektrosk.* **5** 210213
[73] Obikhov-Denisov V V, Sobolev N N and Cheremisinov V P 1960 Vibrational spectra of the modifications of germanium dioxide *Opt. Spektrosk.* **8** 267–70 (in Russian)
[74] Henderson G S, Bancroft G M, Fleet M E and Rogers D J 1985 Raman spectra of gallium and germanium substituted silicate glasses: variations in intermediate range order *Am. Minerals* **70** 946–60

[75] Henderson G S and Fleet M E 1991 The structure of glasses along the Na_2O–GeO_2 join *J. Non-Cryst. Solids* **134** 259–69
[76] Galeener F L and Lucovsky G 1976 Longitudinal optical vibrations in glasses: GeO_2 and SiO_2 *Phys. Rev. Lett.* **37** 1476–8
[77] Pilla O, Fontana A, Caponi S, Rossi F, Viliani G, Gonzalez M A, Fabiani E and Arsamis C P E 2003 Vibrational dynamics of strong glasses: the case of v-SiO_2 and v-GeO_2 *J. Non-Cryst. Solids* **322** 5357
[78] Hubbard B E, Tu J J, Agladze N I and Sievers A J 2003 Optical activity of the boson peak and two-level systems in silica–germania glasses *Phys. Rev.* B **67** 144201
[79] Courtens E, Foret M, Hehlen B, Rufflé B and Vacher R 2003 The crossover from propagating to strongly scattered acoustic modes of glasses observed in densified glasses *J. Phys.: Condens. Matter* **15** S1279–90
[80] Kaiser W, Keck P H and Lange C F 1956 Infrared absorption of oxygen content in silicon and germanium *Phys. Rev.* B **101** 1264–8
[81] Teredesai P V, Anderson D T, Hauser N, Lantzky K and Yager J L 2005 Infrared spectroscopy of germanium dioxide (GeO_2) glass at high pressure *Phys. Chem. Glasses* **46** 345–9
[82] Galeener F L, Leadbetter A J and Stringfellow M W 1983 Comparison of neutron, Raman and infrared vibrational spectra of vitreous SiO_2, GeO_2 and BeF_2 *Phys. Rev.* B **27** 1052–78
[83] Ishihara T, Shirakawa Y, Iida T, Kitamura N, Matsukawa M, Ohtari N and Umesaki N 1999 Brillouin scattering in densified GeO_2 glasses *Japan. J. Appl. Phys.* **38** 3062–5
[84] Durben D J and Wolf G H 1991 Raman spectroscopic study of pressure-induced coordination change in GeO_2 glass *Phys. Rev.* B **43** 2355–63
[85] Polsky C H, Smith K H and Wolf G H 1999 Effect of pressure on the absolute Raman scattering cross section of SiO_2 and GeO_2 glasses *J. Non-Cryst. Solids* **248** 159–68
[86] Magruder R H III, Morgan S, Kinser D L and Weeks R A 1987 Raman studies of the GeO_2 glass preparation history *J. Non-Cryst. Solids* **94** 56–61
[87] Sharma S K, Cooney T F, Wang Z and Van der Laan S 1997 Raman band assignments of silicate and germanate glasses using high-pressure and high-temperature spectral data *J. Raman Spectrosc.* **28** 697–709
[88] Henderson G S and Wang H 2002 Germanium coordination and the germanate anomaly *Eur. J. Minerals* **14** 733–44
[89] Verkhovskii S V, Yakubovsky A Yu, Trokiner A, Malkin B Z, Saikin S K, Ozhogin V I, Tikhomirov A V, Ananyev A V, Gerashenko A P and Piskunov Yu 1999 ^{73}Ge NMR in germanium single crystals with different isotopic composition *Appl. Magn. Reson.* **17** 557–76
[90] Verkhovskii S V, Yakubovsky A Yu, Malkin B Z, Saikin S K, Cardona M, Trokiner A and Ozhogin V I 2003 Isotopic disorder in Ge single crystals probed with ^{73}Ge NMR *Phys. Rev.* B **68** 10421
[91] Takeuchi Y, Nishikawa M and Yammaoto H 2004 High-resolution solid-state ^{73}Ge NMR spectra of hexacoordinated germanium compounds *Magn. Reson. Chem.* **42** 907–9
[92] Stebbins J F, Du L-S, Kroeker S, Neuhoff P, Rice D, Frye J and Jakobsen H J 2002 New opportunities for high-resolution solid-state NMR spectroscopy of oxide materials at 21.1 and 18.8 T fields *Solid State Nucl. Magn. Reson.* **21** 105–15
[93] Du L-S and Stebbins J F 2006 Oxygen sites and network coordination in alkali-germanate glasses and crystals: high-resolution oxygen-17 and sodium-23 NMR *J. Phys. Chem.* B **110** 12427–37
[94] Hussin R, Holland D and Dupree R 1998 Does six-coordinate germanium exist in Na_2O–GeO_2 glasses? oxygen-17 nuclear magnetic resonance measurements *J. Non-Cryst. Solids* **234** 440–5
[95] Jackson I 1976 Melting of the silica isotypes SiO_2, BeF_2 and GeO_2 at elevated pressures *Phys. Earth Planet. Inter.* **13** 218–31
[96] Brazhkin V V and Lyapin A G 2003 High-pressure phase transformations in liquids and amorphous solids *J. Phys.: Condens. Matter* **15** 6059–84
[97] Sharma S K, Virgo D and Kushiro I 1979 Relationship between density, viscosity and structure of GeO_2 melts at low and high pressures *J. Non-Cryst. Solids* **33** 235–48
[98] Duverger C, Turrell S, Bouazaoui M, Tonelli F, Montagne M and Ferrari M 1998 Preparation of SiO_2–GeO_2: Eu^+ planar waveguides and characterization by waveguide Raman and luminescence spectroscopies *Phil. Mag.* B **77** 363–72
[99] Lapeyre C, Petiau J, Calas G, Gauthier F and Gombert J 1983 Ordre local autour du germanium dans les verres du systeme SiO_2–GeO_2–B_2O_3–Na_2O: Etude par spectrometrie d'absorption X *Bull. Minerals* **106** 77–85
[100] Greegor R B, Lytle F W, Kortright J and Fischer-Colbrie A 1987 Determination of the structure of GeO_2–SiO_2 glasses by EXAFS and x-ray scattering *J. Non-Cryst. Solids* **89** 311–23
[101] Schlenz H, Neuefeind J and Rings S 2003 High-energy x-ray diffraction study of amorphous $(Si_{0.71}Ge_{0.29})O_2$ *J. Phys.: Condens. Matter* **15** 4919–26
[102] Henderson G S 2005 The structure of silicate melts: a glass perspective *Can. Mineral.* **43** 1921–58

[103] Du L-S and Stebbins J F 2006 written communication
[104] Sharma S K, Matson D W and Philpotts J A 1984 Raman study of the structure of glasses along the join SiO_2–GeO_2 *J. Non-Cryst. Solids* **68** 99–114
[105] Martinez V, Martinet C and Champagnon B 2004 Light scattering in SiO_2–GeO_2 glasses: quantitative comparison of Rayleigh, Brillouin and Raman effects *J. Non-Cryst. Solids* **345/346** 315–8
[106] Bernard C, Chaussedent S, Monteil A, Balu N, Obriot J, Duverger C, Ferrari M, Bouazaoui M, Kinowski C and Turell S 2001 Application of molecular dynamics techniques and luminescent probes to the study of glass structure: the SiO_2–GeO_2 case *J. Non-Cryst. Solids* **284** 68–72
[107] Nian X, Zhisan X and Decheng T 1989 A Raman study of the ring defects in GeO_2–SiO_2 glasses *J. Phys.: Condens. Matter* **1** 6343–6
[108] Majerus O, Cormier L, Itié J-P, Galoisy L, Neuville D R and Calas G 2004 Pressure-induced Ge coordination change and polyamorphism in SiO_2–GeO_2 glasses *J. Non-Cryst. Solids* **345/346** 34–8
[109] Oeffner R D and Elliott S R 1998 Interatomic potential for germanium dioxide empirically fitted to an *ab initio* surface *Phys. Rev.* B **58** 14791–803
[110] Long D A 1953 Intensities in Raman spectra. I. A bond polarizability theory *Proc. R. Soc.* A **217** 203–21
[111] Tsuchiya T, Yamanaka T and Matsui M 2000 Molecular dynamics study of pressure induced transformation of quartz-type GeO_2 *Phys. Chem. Minerals* **27** 149–55
[112] Bingelli N, Chelikowsky J R and Wetzcovitch R M 1994 Simulating the amorphization of α-quartz under pressure *Phys. Rev.* B **49** 9336–40
[113] Grismditch M, Polian A, Brazhkin V and Balitskii D 1998 Elastic constants of α-GeO_2 *J. Appl. Phys.* **83** 3018–20
[114] Van Hoang V 2006 Static and dynamic properties of simulated liquid an amorphous GeO_2 *J. Phys.: Condens. Matter* **18** 777–86
[115] Kim D, Kawamura K, Enomoto N and Nakagawa Z 1996 Reproduction of pressure-induced structural transformation of α-quartz-type GeO_2 in molecular dynamics simulations *J. Ceram. Soc. Japan* **104** 10971099
[116] Nanba T, Miyaji T, Takada J, Osaka A, Miura Y and Yasui I 1994 Computer simulation on the structure and vibrational spectra in Ge–Pb–O–F glass *J. Non-Cryst. Solids* **177** 131–6
[117] Wefing S 1999 Modeling of continuous random networks: a case study for vitreous GeO_2. I. Model generation *J. Non-Cryst. Solids* **244** 89–111
[118] Araujo R 1996 Oxygen vacancies in silica and germania glasses *J. Non-Cryst. Solids* **197** 164–9
[119] Guttierez G and Rogan J 2004 Structure of liquid GeO_2 from a computer model *Phys. Rev.* E **69** 031201
[120] Giovambattista N, Stanley E G and Sciortino F 2005 Phase diagram of amorphous solid water: Low-density, highdensity, and very-high-density amorphous ices *Phys. Rev.* E **72** 031510
[121] Van Hoang V 2006 Anomalous diffusion in simulated liquid GeO_2 *Physica* B at press
[122] Micoulaut M 2004 A comparative numerical study of liquid GeO_2 and SiO_2 *Chem. Geol.* **213** 197–205
[123] Rustad J R, Yuen D A and Spera F J 1991 The sensitivity of physical and spectral properties of silica glass to variations in interatomic potentials under high pressures *Phys. Earth Planet Inter.* **65** 210–30
[124] Richet P 1990 GeO_2 vs SiO_2: glass transitions and thermodynamic properties of polymorphs *Phys. Chem. Minerals* **17** 79–88
[125] Kiczenski T J, Chris Ma, Hammarsten E, Wilkerson D, Affatigato M and Feller S 2000 A study of selected physical properties of alkali germanate glasses over wide ranges of composition *J. Non-Cryst. Solids* **272** 57–66
[126] Vashishta P, Kalia R K and Ebbsjo I 1989 Structural correlations and phonon density of states in $GeSe_2$: a molecular dynamics study of molten and amorphous states *Phys. Rev.* B **39** 6034–46
[127] Vollmayr K, Kob W and Binder K 1996 Cooling rate effects in amorphous silica: a computer-simulation study *Phys. Rev.* B **54** 15808–27
[128] Sipp A, Bottinga Y and Richet P 2001 New viscosity data for 3d network liquids and new correlations between old parameters *J. Non-Cryst. Solids* **288** 166–74
[129] Horbach J and Kob W 1999 Static and dynamic properties of a viscous silica melt *Phys. Rev.* B **60** 3169
[130] Tokuda T and Kingery W D 1963 Oxygen diffusion and vaporization rates for liquid and solid germanium dioxide *J. Appl. Phys.* **34** 2104–5
[131] Glasstone S, Laider K J and Eyring H 1941 *The Theory of Rate Processes* (New York: McGraw Hill)
[132] Smith K H, Shero E, Chizmeshya A and Wolf G H 1995 The equation of state of a polyamorphic germania glass: a two-domain description of the viscoelastic response *J. Chem. Phys.* **102** 6851–7
[133] Birch F 1952 Elasticity and constitution of the earths interior *J. Geophys. Res.* **57** 227–86
[134] Dingwell D B, Knoche R and Webb S L 1993 A volume temperature relationship for liquid GeO_2 and some geophysically relevant derived parameters for network liquids *Phys. Chem. Minerals* **19** 445–53

[135] Alejandre J, Tildesley D J and Chapela G A 1995 Molecular dynamics simulation of the orthobaric densities and surface tension of water *J. Chem. Phys.* **102** 4574–83
[136] Trachenko K O, Dove M T, Brazhkin V and El'kin F S 2004 Network rigidity and properties of SiO_2 and GeO_2 under pressure *Phys. Rev. Lett.* **93** 135502
[137] Trachenko K O 2006 private communication
[138] Wegner F J 1972 Corrections to scaling laws *Phys. Rev.* B **5** 4529–36
[139] Micoulaut M and Guissani Y 2005 unpublished
[140] Guissani Y 2006 private communication
[141] Sugai S, Sotokawa H, Kyokane D and Onodera A 1996 Bose peak in the Raman spectra of densified SiO_2 and GeO_2 glass under high pressure *Physica* B **219/220** 293–5
[142] Shanavas K V, Nandini G and Sharma S M 2006 Classical molecular dynamics simulation of behavior of GeO_2 under high pressures and at high temperatures *Phys. Rev.* B **73** 094120
[143] Micoulaut M, Yuan X and Hobbs L W 2006 Coordination and intermediate range order alterations in densified networks *J. Non-Cryst. Solids* submitted
[144] Trachenko K O, Dove M T, Hammonds K D, Harris M J and Heine V 1998 Low energy dynamics and tunneling states in silica glass *Phys. Rev. Lett.* **81** 3431–4
[145] Trachenko K O, Dove M T, Harris M J and Heine V 2000 Dynamics of silica: two-level tunneling states and low-energy floppy modes *J. Phys.: Condens. Matter* **12** 8041–64
[146] Thorpe M F and Duxburry P M 1999 *Rigidity Theory and Applications* (New York: Plenum/Kluwer Academic)
[147] Selvenathan D, Bresser W J and Boolchand P 2000 Stiffness transition in Si_xSe_{1-x} glasses from Raman scattering and temperature modulated differential scanning calorimetry *Phys. Rev.* B **61** 15061–76
[148] Boolchand P, Georgiev D G and Goodman B 2001 Discovery of the intermediate phase in chalcogenide glasses *J. Optoelectron. Adv. Mater.* **3** 703–20
[149] Tsiok O B, Brazhkin V V, Lyapin A G and Khvostantsev L G 1998 Logarithmic kinetics of the amorphous–amorphous transformations in SiO_2 and GeO_2 glasses under high pressure *Phys. Rev. Lett.* **80** 999–1002
[150] Polian A and Grimsditch M 1990 Room-temperature densification of a-SiO_2 versus pressure *Phys. Rev.* B **41** 6086–7
[151] Christie D M and Chelikowsky J R 2000 Electronic and structural properties of germania polymorphs *Phys. Rev.* B **62** 14703–11
[152] Murnhagan F D 1944 The compressibility of media under extreme pressures *Proc. Natl Acad. Sci. USA* **30** 224247